Doctoral Dissertation

Voltage Control of Fluorescence Protein Emissions at the Metal-Solution Interface

TRISHA FARHA DIBA

Supervisor: HIDEKAZU TSUTSUI

Graduate School of Advanced Science and Technology

Japan Advanced Institute of Science and Technology

Materials science

June 2023

Table of Content

Abstract

Numerous natural proteins that emit fluorescence have been discovered from various organisms, and their genetically engineered variants have been generated in the last several decades. A variety of physicochemical phenomena exhibited by fluorescence proteins have been utilized to develop many key technologies in life science over the last few decades. Accordingly, the physicochemical properties of fluorescence proteins have been deeply investigated in the bulk solution that mimics the cellular environment, but those at the less common environment such as surface and interface have not been deeply investigated. In this research work, it was found that the fluorescence protein exhibits voltage-dependent photoluminescence after its immobilization on the metal-solution interface. Upon the blue light photoexcitation, a yellow-emitting, version of green fluorescence protein (GFP), called Venus was immobilized on the gold electrode surface, robust enhancement or decrease of fluorescence was induced by applying negative or positive bias, respectively. This previously unappreciated phenomenon was then implemented as a protein-based microdisplay. Several experiments have been done to

solve the mechanism for cathodic enhancement utilizing the characteristic optical properties in the three different fluorescence proteins. From the simultaneous electrochemical and fluorescence measurements in Venus, a solid correlation was found between the modulation of fluorescence and current reflecting cathodic hydrogen evolution, which led to a hypothesis that shift in the protonation-deprotonation equilibrium of the chromophore driven by hydrogen evolution at the metal surface underlies the phenomena. The hypothesis predicted that voltage dependency should be also found in the photoconversion from green to red of fluorescence protein which is known as a protonation-dependent process. The hypothesis was verified by observing clear voltage dependency for the photoconversion in Kikume Green - Red (KikGR), an engineered photoconvertible fluorescence protein, at the interface. Later experiments have been done to address how the shift in protonation equilibrium is driven by hydrogen evolution. The analysis using iR-pHluorin, a fluorescence protein variant with the inverse pH-sensitivity revealed that there exists an interface-specific mode of protonation-

deprotonation reaction, and where the protonation equilibrium is directly coupled to the cathodic hydrogen evolution.

The interface-specific mode is distinct from that conventionally seen in protein in the bulk solution and there the protonation patterns of the constituent titratable residues are determined through the acid-base equilibrium of the local environment. Interface-specific mechanism-based possible applications are then discussed, including monitoring of hydrogen evolution reactions at near neutral conditions.

Keywords:

Fluorescence protein, Photoluminescence, Imaging, Protonation-deprotonation, Hydrogen Evolution Reaction (HER).

Chapter 1

General Introduction

1.1. Fluorescence

Some substances can emit light with longer wavelength after the absorption of light or other electromagnetic radiation with shorter wavelength. And this process is called fluorescence [1-2].

1.1. Fluorescence Protein

Fluorescence proteins are a special category of protein that has the extraordinary characteristic of the formation of visible wavelength chromophore autonomously within their own amino acid sequence.

Green Fluorescence Protein (GFP) was the first fluorescence protein which was isolated from jellyfish *Aequorea victoria*. From other organisms such as sea anemones, corals, copepods, zoanithids, and from lancelets fluorescence proteins can also be found [3-4].

1.3. Discovery and history of fluorescence proteins

The first fluorescence protein GFP which glowed bright green under ultraviolet light was discovered in the early 1960s by scientist Osamu Shimomura. He isolated GFP from the *Aequorea victoria* because of his huge interest in bioluminescence [5].

1.4. History

After the discovery of GFP in the early 1960s by scientist Osamu Shimomura, he established the structure of GFP which is responsible for the special characteristics of GFP by 1979. Through the GFP gene cloning by 1992 the full sequence of GFP was accomplished by Ward and Prasher in Cormier's laboratory [6]. Next GFP was first expressed by Chalfie's group in E. coli and glowing green cultures were produced which indicate that this unique protein can be utilized as a fluorescent marker in vivo condition. By 1994 it has been determined that the GFP expression can be accomplished in the touch neurons of Caenorhabditis elegans [7] and created a new era in biological science. Later Tsien also worked on the development of the biosensor function of fluorescent proteins, such as pH sensors. Next many other variants of fluorescence proteins have been engineered genetically which has a huge use in life sciences.

1.5. Green Fluorescence Protein (GFP)

Under blue to ultraviolet light Green Fluorescence Protein (GFP) shows bright green fluorescence . Its major and minor excitation peak are at a wavelength of 395 nm and 475 nm respectively with emission peak is at 509 nm.

The molecular weight of GFP is 27 kD protein which have 238 amino acid residues. Its

molecular structure was first determined by using X-ray crystallography in 1996 [8-10]. The crystal structure of GFP is an 11-stranded βbarrel, threaded by an α-helix (Figure 1). There are 9 to 13 amino acid residues in each beta strand and hydrogen bonds with adjoining beta strands create compact structure. The dimensions of β-barrel structure is approximately 25 Å × 40 Å, and due to dense amino acid residues packing in GFP, it display a huge stability. The GFP chromophore is in the α-helix. The chromophore is situated very close to the center of the can-like cylinder. In GFP sequence residues 65-67 (Ser-Tyr-Gly) automatically form the chromophore p-hydroxybenzylideneimidazolinone [11-13]. GFP has great resistance to changes in temperature, pH, and many types of denaturing agents because of its compact structure.

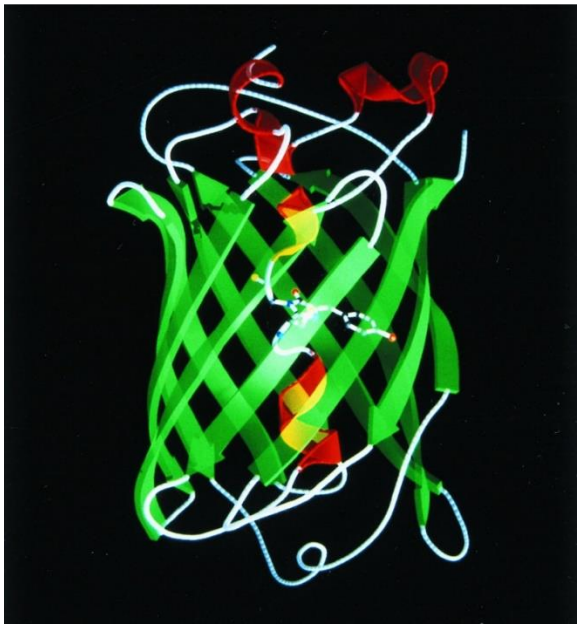

Figure 1: Tertiary structure of GFP [10].

1.6. Effect of pH on Green Fluorescence Protein (GFP)

From pH 6-10 the fluorescence of wild-type GFP is stable, but fluorescence decreases at pH< 6 and increases from pH 10-12 [14]. Some experiments have shown that some variants of GFP such as EGFP show more pH sensitivity [15-16]. Due to the protonation and deprotonation of certain important amino acid residues within the chromophore of GFP the pH sensitivity is caused. GFP mutants can be genetically fused with certain targeting motifs and the pH of diverse cellular environment can be measured.

1.7. Chromophore variations

The most interesting part of a fluorescence protein is its chromophore. By the process called cyclization at positions 65–67 (Ser-Tyr-Gly) of the GFP backbone the chromophore of GFP is formed. Strong changes in spectral characteristics happened after the ionization of the chromophore's Tyr66 phenolic hydroxyl group. The chromophore in wild type GFP is in equilibrium between protonated (neutral) and deprotonated (anionic) states. GFP chromophore in the protonated state absorbs at ~400 nm and at ~460 nm can effectively emit blue light. Most often, GFP-like chromophore in its protonated state undergo a procedure called ESPT (exited state proton transfer): just after the excitation, the chromophore becomes charged after loses one of its protons, thus scattering a part of the absorbed energy [17-18] and eventually, it emits green fluorescence.

1.8. GFP derivatives

Because of the enormous usage and the expanded needs of scientists, various GFP mutants have been made by genetic engineering process [19-20]. Over the years, GFP and their derivatives have become useful tools for understanding different biological processes intracellularly.

1.9. Yellow fluorescence protein (YFP)

One type of GFP genetic mutant is YFP. This mutation occurs due to the substitution of threonine with tyrosine at 203 residue position. YFP excitation and emission peak is 513 and 527 nm respectively 527 nm [21-22]. YFP and YFP derivatives display an important environmental sensitivity due to their absorbance level [23]. YFP fluorescence depends on pH and thus it acts as a good pH sensor [23]. Citrine, a less sensitive YFP variant was developed later [24], citrine. With reduced pH dependence a different YFP variant has been developed recently [25]. Yellow emission variants of green fluorescent protein (GFP) have been found useful in a variety of applications in biological systems. Due to its separable characteristic of the excitation and emission peaks, YFP has become an important tool in molecular biology.

1.10. Enhanced cyan fluorescence Protein.

Cyan fluorescent protein (CFP) is another kind of GFP variant [26]. Cyan color Fluorescence emission that is mainly obtain by the mutation of the central residue of GFP chromophore that is tyrosine into a tryptophan, and caused enhanced cyan fluorescence protein (ECFP), which is the first cyan fluorescence protein which can be used for various purposes (CFP) [26]. For the measurement of intracellular pH many tools have been developed [27-28]. Enhanced cyan fluorescence protein (ECFP) acts as a

satisfactory pH sensor due to their powerful pH sensitivity [29-30]. CFP can be used as a biological marker.

1.11. pHlourins

Another pH sensitive variant of GFP is pHluorin which can be used to examine the pH of the different cell organelles such as mitochondria, cytosol, and others [31-33].

1.12. Keima-Red

Dimeric Keima-Red (dKeima-Red) and monomeric Keima-Red (mKeima-Red) are unique fluorescence proteins that emit red light at 616 and 620 nm respectively with an absorption peak at 440 nm. Keima- Red can be used in fluorescence spectroscopy such as FCCS (fluorescence cross-correlation spectroscopy) [34-35].

1.13. Photoconvertible fluorescence protein

Photoconvertible fluorescence protein can shift their emission color from green to red irreversibly when exposed to blue color. A natural photoconvertible fluorescence protein named Kaede can be found in the coral *Trachyphyllia geoffroyi* [36-37]. This protein was named Kaede according to the leaves of Japanese maple trees which can turn their color

from green to red in autumn. KikG is another photoconvertible protein, which can be obtained from a third stony coral, Favia favus [38-40].

1.14. Some applications of fluorescence proteins

Green fluorescence protein and its derivatives have great application in cell biology. Its gene cloning and heterologous expression cause its growing use [41-42]. It has a great use as fusion tags, reporter gene and GFP biosensor [43-44].

References

1. Lagorio MG, Cordon GB, Iriel A. 2015 Reviewing the relevance of fluorescence in biological systems. Photochem. Photobiol. Sci. 14, 1538– 1559. (doi:10. 1039/C5PP00122F)
2. Vukusic P, Hooper I. 2005 Directionally controlled fluorescence emission in butterflies. Science 310, 1151. (doi:10.1126/science.1116612).
3. Field SF, Bulina MY, Kelmanson IV, Bielawski JP, Matz MV. Adaptive evolution of multicolored fluorescent proteins in reef-building corals. J Mol Evol 62: 332–339.2006
4. Craig, J., Jamieson, A. J., Bagley, P. M. & Priede, I. G. Naturally occurring bioluminescence on the deep-sea floor. J. Mar. Sys. 88, 563–567 (2011).
5. O. Shimomura, F.H. Johnson, and Y. Saiga, J. Cell. Comp. Physiol. 59, 223 (1962).
6. Prasher, D. et al. (1992) Gene 111 229-233.
7. Chalfie, M. et al. (1994) Science 263 802-805.
8. Ormö, M. et al. (1966) Science 273 1392-1395.
9. Yang F, Moss LG, Phillips GN., Jr *Nat Biotechnol.* 1996;14: 1246–1251.
10. Brejc, K. et al. (1997) Proc. Natl. Acad. Sci. USA 94 2306-2311.
11. Heim R, Prasher DC, Tsien RY. 1994. Proc. Natl. Acad. Sci. USA 91:12501–4
12. Cubitt AB, Heim R, Adams SR, Boyd AE, Gross LA, Tsien RY. 1995. Trends Biochem. Sci. 20:448–55
13. Tsien, R. (1998) Annu. Rev. Biochem. 67 509-544.
14. Ward, W.W. 1981. Properties of the coelenterate green-fluorescent proteins. In: Bioluminescence and Chemiluminescence: Basic Chemistry and Analytical

Applications. DeLuca, M.A. and McElroy, W.D., eds, Academic Press, New York, pp. 235-242.

15. Kneen, M., Farinas, J., Li, Y., and Verkman, A.S. 1998. Green fluorescent protein as a noninvasive intracellular pH indicator. Biophys. J. 74: 1591- 1599.
16. Llopis, J. et al. (1998) Measurement of cytosolic, mitochondrial, and Golgi pH in single living cells with green fluorescent proteins. Proc. Natl. Acad. Sci. U. S. A. 95, 6803–6808.
17. Chattoraj M., King, B.A., Bublitz, G.U., and Boxer, S.G. 1996. Ultra-fast excited-state dynamics in green fluorescent protein: Multiple states and proton transfer. *Proc. Natl. Acad. Sci.* 93**:** 8362–8367.
18. Lossau H., Kummer, A., Heinecke, R., Pollinger-Dammer, F., Kompa, C., Bieser, G., Jonsson, T., Silva, C.M., Yang, M.M., Youvan, D.C., et al. 1996. Time-resolved spectroscopy of wild-type and mutant green fluorescent proteins reveals excited-state deprotonation consistent with fluorophore–protein interactions. *Chem. Phys.* 213**:** 1–16.
19. haner NC, Steinbach PA, Tsien RY (Dec 2005). "A guide to choosing fluorescent proteins" (PDF). *Nature Methods*. **2** (12): 905-909
20. Wilhelmsson M, Tor Y (2016). *Fluorescent Analogs of Biomolecular Building Blocks: Design and Applications*. New Jersey: Wiley. ISBN 978-1-118-17586-6.
21. - Wachter, R. M., Yarbrough, D. Y., Kallio, K., and Tsien, R. Y. (2000) J. Mol. Biol. 301, 157–171
22. Wachter, R. M., Elsliger, M.-A., Kallio, K., Hanson, G. T., and Remington, S. J. (1998) Structure (Lond.) 6, 1267–1277.

23. Takahashi, A., Zhang, Y., Centonze, E., and Herman, B. (2001) BioTechniques 30, 804–812

24. Griesbeck, O., Baird, G. S., Campbell, R. E., Zacharias, D. A., and Tsien, R. Y. (2001) J. Biol. Chem. 276, 29188–29194

25. Nagai, T., Ibata, K., Park, E. S., Kubota, M., Mikoshiba, K., and Miyawaki, A. (2002) Nat. Biotechnol. 20, 87–90.

26. Heim R, Tsien RY. 1996 Engineering green fluorescent protein for improved brightness, longer wavelengths and fluorescence resonance energy transfer. Curr. Biol. 6, 178– 182. (doi:10.1016/ S0960-9822(02)00450-5)

27. Roos A, Boron WF (1981) Intracellular pH. Physiol Rev 61 (2):296–434

28. Han J, Burgess K (2010) Fluorescent indicators for intracellular pH. Chem Rev 110(5):2709–272

29. Villoing A, Ridhoir M, Cinquin B, Erard M, Alvarez L, Vallverdu G, Pernot P, Grailhe R, Merola F, Pasquier H (2008) Complex fluorescence of the cyan fluorescent protein: comparisons with the H148D variant and consequences for quantitative cell imaging. Biochemistry 47(47):12483–12492.

30. Fredj A, Pasquier H, Demachy I, Jonasson G, Levy B, Derrien V, Bousmah Y, Manoussaris G, Wien F, Ridard J, Erard M, Merola F (2012) The single T65S mutation generates brighter cyan fluorescent proteins with increased photostability and pH insensitivity. PLoS One 7(11): e49149

31. Rossano, A. J., Chouhan, A. K. & Macleod, G. T. Genetically encoded pH-indicators reveal activity-dependent cytosolic acidification of Drosophila motor nerve termini in vivo. J. Physiol. 591, 1691–1706 (2013).

32. Redhu, A. K. et al. pHluorin enables insight into the transport mechanism of antiporter Mdr1: R215 is critical for Drug/H+ antiport. Biochem. J. 473, 3127–3145 (2016).
33. Marešová, L., Hošková, B., Urbánková, E., Chaloupka, R. & Sychrová, H. New applications of pHluorin - Measuring intracellular pH of prototrophic yeasts and determining changes in the buffering capacity of strains with affected potassium homeostasis. Yeast 27, 317–325 (2010).
34. Kettling, U., Koltermann, A., Schwille, P. & Eigen, M. Real-time enzyme kinetics monitored by dual-color fluorescence cross-correlation spectroscopy. Proc. Natl. Acad. Sci. USA 95, 1416–1420 (1998).
35. Kohl, T., Haustein, E. & Schwille, P. Determining protease activity in vivo by fluorescence cross-correlation analysis. Biophys. J. 89, 2770–2782 (2005).
36. Ando R, Hama H, Yamamoto-Hino M, Mizuno H, Miyawaki A (2002) An optical marker based on the UV-induced green-to-red photoconversion of a fluorescent protein. *Proc Natl Acad Sci USA* 99: 12651–12656.
37. Mizuno H, Mal TK, Tong KI, Ando R, Furuta T, Ikura M, Miyawaki A (2003) Photo-induced peptide cleavage in the green-to-red conversion of a fluorescence protein. ***Mol Cell* 12**: 1051–1058.
38. Kulesa PM, Teddy JM, Stark DA, Smith SE, McLennan R: Neural crest invasion is a spatially-ordered progression into the head with higher cell proliferation at the migratory front as revealed by the photoactivatable protein, KikGR. Dev Biol. 2008, 316: 275-87. 10.1016/j.ydbio.2008.01.029.

39. Tsutsui H, Karasawa S, Shimizu H, Nukina N, Miyawaki A: Semi-rational engineering of a coral fluorescent protein into an efficient highlighter. EMBO Rep. 2005, 6: 233-8. 10.1038/sj.embor.7400361.

40. Wiedenmann J, Ivanchenko S, Oswald F, Schmitt F, Rocker C, Salih A, Spindler KD, Nienhaus GU (2004) EosFP, a fluorescent marker protein with UV-inducible green-to-red fluorescence conversion. *Proc Natl Acad Sci USA* 101: 15905–15910.

41. Bastiaens, P. I. H.; Pepperkok, R. Trends Biochem. Sci. 2000, 25, 631-637. 42.

42. Lippincott-Schwartz, J.; Snapp, E.; Kenworthy, A. Nat. Rev. Mol. Cell Biol. 2001, 2, 444-456.

43. Doi N, Yanagawa H. Design of generic biosensors based on green fluorescent proteins with allosteric sites by directed evolution. Febs Letters. 1999;453:305–307.

44. Zhong JQ, Freyzon Y, Ehrlich DJ, Matsudaira P. Enhanced detection sensitivity using a novel solid-phase incorporated affinity fluorescent protein biosensor. Biomol Eng. 2004;21:67–72.

Chapter 2: Discovery

Voltage control of fluorescence protein emissions at the metal-solution interface

Chapter 2 Key Points

- A phenomenon was discovered in which fluorescence protein immobilized at the gold-solution interface exhibits voltage regulated modulation of fluorescence emission.

- Negative and positive voltage applied to the gold electrode elicited robust increase and decrease of fluorescence, respectively.

- Fluorescence protein based micro-display employing the voltage regulated modulation of fluorescence emissions was successfully fabricated and operated.

- The pilot experiment using a fluorescence protein variant suggested that the fluorescence modulation is likely neither driven through local pH change, distance change associated with electrostatic attraction-repulsion, nor change in the emission spectrum.

- Mechanism for the fluorescence modulation remained unsolved.

Introduction

Several natural proteins that emit fluorescence have been discovered from various organisms, and their genetically engineered variants have been generated in the last several decades. Iconic examples include the green fluorescence protein (GFP) from jellyfish (1-3), the phycobiliproteins from cyanobacteria and algae (4), and the bilirubin-binding fluorescence protein from eels (5). These proteins exhibit a wide variety of physiochemical phenomena which have been utilized to develop many key technologies in the life-science field. For example, förster resonance energy transfer between a pair of proteins has been successfully exploited to visualize spatiotemporal progressions of intermolecular interactions in live cells (6, 7); and the photo-switching behavior found in certain kinds of proteins has been used not only as a molecular tag but also used in the super-resolution microscopy techniques (8-12). In this regard, their physicochemical properties in “bulk” solutions mimicking the cellular environments have been the major focus of the fluorescence protein research, and those at rather uncommon environments such as “surface” and “interface” have been only occasionally explored (13, 14). In this chapter, we describe our discovery of a previously unappreciated phenomenon of fluorescence protein which takes place at the interface between metal and solution.

It was found that emission from fluorescence proteins immobilized at metal-solution interface is robustly modulated by changing metal potential with respect to the solution, which we came across during establishing experimental protocols for electrostatic protein depositions to metal substrates. We then implemented this phenomenon in a prototype micro-display device.

Materials and Methods

Fabrication of the microelectrode chamber

A borosilicate glass substrate (22 x 32 mm, Matsunami, Osaka) was sputtered with chromium and gold using an ion beam sputtering system (EIS-220, Elionix, Tokyo). Sputtering conditions were as follows: Ar pressure 6 x 10^{-3} PA, microwave power 1000W, acceleration voltage 1000V, ion emission current 0.6 A. Sputtering was performed for 20- and 40-min using Cr and Au target, which resulted ~ 30 nm and ~ 200 nm thickness, respectively. Electrode lines and connection pads were then patterned by conventional photolithography. Onto that, an additional layer of epoxy-based photoresist (thickness ~5 μm, SU-8 3005; MicroChem, MA, USA) was patterned to form the insulator and electrode openings. After hard baking (200°C; 10 min), a glass-ring (ϕ 20 mm; 5 mm height) was attached using poly-dimethylsiloxane elastomer to compose a solution

chamber. The whole chamber was plasma-cleaned before use (PDC-32G, Harrick Plasma, N.Y., USA).

Electrostatic protein deposition onto metal surface

Protein of interest was electrostatically deposited onto the gold electrode surface by applying voltage pulses using a source measurement unit (Keithley 2401). Eight different proteins were used in this study. A yellow variant of GFP (YFP), a cyan variant (CFP), iR-pHluorin, circular permuted GFP, a fusion protein of YFP and Fc domain (YFP-Fc), and a fusion protein of NanoLuc and GFP (NanoLuc-GFP) were prepared in house by the standard affinity purifications following recombinant expressions either in Escherichia coli (JM109 strain) or human embryonic kidney cells. Protein-A (TCI chemicals, Tokyo) and streptavidin Alexa 488 (Thermo Fisher Scientific, MA, USA) were commercially purchased. Protein solution was prepared at 0.1 mg/ml in 20mM HEPES (pH 9.0) containing 1mM NaCl and 0.05% Triton-X surfactant. The estimated Debye length was ~2.4 nm. The high pH and surfactant were essential to keep protein negatively charged and to avoid non-specific adsorption, respectively.

Microscopy

Fluorescence images were acquired using a microscope (MVX10, Olympus) equipped with a stable xenon lamp (Ushio, Tokyo) and a CCD camera (OrcaR2; Hamamatsu Photonics, Hamamatsu). A scheme of the light path is shown in Fig. 1c. The excitation filters, dichroic mirrors, emission filters used were 490-500, 515YFP, 515-560 (Olympus) for the detections of YFP and iR-pHuorin; 438/24, FF458, 483/32 (Semrock) for CFP; and 460-480, 490GFP, 495-540 (Olympus) for circular permutated GFP and Alexa 488 fluorophore. Data was analyzed using custom made software written in IDL (Research Systems, USA) and Image-J (NIH, USA).

Results

Electrostatic deposition of protein at the gold-solution interface

In our laboratory, we were trying to launch a new research project to immobilize functional biomolecules on micro-metal electrodes and then detect their interactions with live nerve cells and the resulting electronic currents associated with neural activities. The finding described in this chapter was unexpectedly encountered during the establishment of the immobilization protocol for the above-mentioned project. **Figure 1** shows an example of gold microelectrode chamber used in these experiments, which was fabricated

through the conventional chromium and gold sputtering onto the glass substrate and subsequent photolithography (**Fig. 1 a, b**). Typically, the experimental chamber consisted of ~16 microelectrodes with circular openings of ~50 um diameter (**Fig. 1c**).

It was found that protein is immobilized onto the gold electrode in one-step upon the application of voltage pulses between the gold electorode (+) and Ag/AgCl electrode (-) in the bath solution containing protein of interest. Protein immobilization was assayed after replacing protein solution into the protein free experiment buffer, which consisted of 1mM NaCl and 20mM HEPES (adjusted with NaOH to pH7.4) unless otherwise noted (**Fig. 2a, b**). Figure 2c shows an example of immobilization of Protein A, which is a protein that originates from the bacteria *Staphylococcus aureus* and has a binding affinity for the Fc domain of immunoglobulins. In this example, deposition was carried out by applying different number of 100 ms square voltage pulses of 1.7 V amplitude. After washing out of protein solution, the electrode chamber was incubated with apparently excess amount of Fc-YFP fusion protein in PBS (phosphate buffered saline) containing 0.01% Triton-X. Triton-X was used to prevent non-specific bounding of Fc-YFP to the experimental chamber, and then was again rinsed with PBS. From YFP fluorescence image, it was found that the amount of protein immobilized in this method is well controllable by the number of voltage pulse to apply (**Fig. 2c**). Furthermore, to test

the stability of the binding of protein A – metal surface, fluorescence was re-examined after keeping the whole electrode chamber at 37°C for 3 days. Comparable intensity of YFP fluorescence was still detectable even after 3 days, which showed the sufficient binding stability of this method (**Fig. 2d**). It was also possible to immobilize different kind of proteins to specific electrode sites by repeating the electrostatic deposition and rinse process. **Figure 2e** shows an example of sequential depositions of YFP and CFP in the two diagonal electrodes.

Finding of the interface effect

It was tested from a simple curiosity whether the fluorescence emission is sensitive to electrode potential. To this end, fluorescence imaging was performed using YFP immobilized microelectrodes in the experimental buffer consisting of 20mM HEPES (pH 7.4) and 1mM NaCl (**Fig. 3a**). Then, in response to the applied potential, unambiguous modulation of YFP fluorescence was observed. Fluorescence was robustly enhanced or decreased upon negative or positive electrode potentials, respectively. **Figure 3b** shows an example of fluorescence responses elicited by the voltage step to -1.25 or -1.5 V and then recovery to null potential (0 V). **Figure 3c** shows representative fluorescence

modulations as a function of time elicited by the 0.5 sec voltage steps with several different amplitudes ranging from -1.5V to +1.5V.

Repeatability

This phenomenon showed high repeatability. **Figure 4** shows a result of stability test in which a single YFP immobilized microelectrode was subject to 100 iterations of applying negative voltage pulses (-1.5V, 0.5sec) in the total 260 sec imaging time.

GFP based micro-display

Motivated by the high repeatability of the modulation phenomenon, a prototype micro-scale (240 x 460 μm) seven-segment display device was fabricated (**Fig. 5a**). The electrodes composing the pixels were again deposited with YFP. The electrode potential to turn on and off pixels were set at -1.5 V and +1.25 V (v.s. Ag/AgCl), respectively, and were applied though a BCD-to-seven-segment decoder (HD74HC4511, Hitachi), multiplexer (TC4053BP, Toshiba), and a pulse generator (AWG-50, Elmos, Osaka). Successful operations of the device as in the example shown in **Figure 5b**. Operation currents were in the range of ~ 10^{-6} A per a pixel.

Response from the other proteins

It was then aimed to gain some insights into the potential mechanism. First, a possibility was tested in which the fluorescence modulation is simply due to local pH change at the interface. Although generations of electrolytic gas bubbles were not clearly noticeable in the current condition, theoretically, there could be changes in local pH due to the unperceived level of water electrolysis. Especially, YFP fluorescence depends on protonation state of the phenolic hydroxyl group of the chromophore (2). In the test of CFP which does not contain the phenolic group in its chromophore (2), clear modulations were still evident showing that the phenolic group is not requisite (**Fig. 6a**). Yet local pH change was not necessarily excluded because CFP still has pH-sensitivity of the same direction as in YFP (i.e., dimmer at lower pH) likely due to pH-dependent chromophore isomerization (18). So iR-pHluorin was tested which exhibits the reverse pH-sensitivity: brighter at lower pH (19). If it is assumed that change in local pH is the cause, YFP and iR-pHluorin should show modulations of opposite directions. However, the direction was unaffected in the experiment (**Fig. 6b**), thus excluding the local pH change as the major cause for the interface effect. We tested two types of proteins as well, circular-permuted GFP and streptavidin conjugated with Alexa-488 fluorophore, to address whether the interface effect is just specific to the GFP-like beta-barrel proteins. The present effect

seemed to be a more general phenomenon since clear modulations were observed in both cases (**Fig. 6c, d**).

It has been revealed that interaction between the incident excitation light and the metal surface could influence the electric field felt by the fluorophore nearby. We next addressed this possibility using NanoLuc-GFP, a fusion protein of bioluminescent NanoLuc protein . This protein emits in the presence of NanoLuc substrate, furimazine, without the need for excitation light. The optical filters in the imaging light-path were omitted to detect emission from the entire spectrum region. We observed that, in the absence of excitation light, the emission still exhibited unambiguous modulations, increasing upon negative potential and decreasing upon positive potential (**Fig. 6e**). Summarizing the above, the series of experiments using eight different proteins revealed that the present interface effect is not specific to GFP-like protein, not due to local pH change at the metal surface, and nor to the interaction between the excitation light and metal. While the minor differences among the signals might reflect some properties specific to these proteins, they all exhibited modulations in the same direction. These observations thus suggested that the modulation occurs not simply due to changes in the local environment but more likely due to the metal-protein interactions, where possible effects may include distance dependent energy transfer, charge transfer, change in non-radiative decay rate, as well as

structural deformations.

Some additional experiments aiming to gain insights for the mechanism

Aiming to further narrow down the possibilities for the mechanism, we carried out additional characterizations using YFP. First, whether the energy gap between the excited and ground states is affected during the modulations was addressed by measuring emission spectra using a fiber optic spectrophotometer (USB4000, Ocean Optics). The view was not supported because of the non-significant difference between at 0 and 1.25 V (v.s. Ag/AgCl) (**Fig. 7a**). One clear feature of the present interface effect is its relatively slow response time which is typically in the scale of a second. So, we next performed a simple experiment of varying the timings of shutter opening for excitation light to address whether the metal potential effect proceeds in the absence of excitation light. We found that comparable signal developed irrespective of the timing of initiating photo-excitation (**Fig. 7b**), thus suggesting that the metal potential can at least affect the fluorescence proteins in the ground state.

One straightforward hypothesis consistent with the observations so far may be that the protein-metal distance could be electrostatically altered by the metal potential, affecting the rate of resonance energy transfer between the metal and proteins. Theoretically, from the isoelectric point of YFP in solution (pI = 5.7), YFP is negatively charged at pH 7.4 of

the current experimental condition. So, the model is reasonable considering that the metal-protein distance could increase upon negative electrode potential, decreasing energy transfer rate, and vice versa upon positive potential. One simple experiment would be to see the response at pH below the isoelectric point, where the protein is positively charged theoretically and so the direction of the signal is expected to become opposite to that at pH 7.4. In the experiment, however, the direction was still unaffected at pH 5.0 (**Fig. 7c**). It is worthwhile to mention that because there remains a possibility that the isoelectric point of proteins deposited onto the metal can differ from that in the bulk solution, the hypothesis of distance-change remained tentative.

Finally, we studied YFP-Fc bound to the deposited protein-A layer to ask whether the direct adsorption of fluorescence emitting protein to the metal is essential or not (**Fig. 2c, Fig. 7d**). If direct charge transfer between metal and protein is significant, immobilization via the intermediate Protein-A is expected to attenuate the electric-field effect. In the experiment, however, the modulation was still unambiguous (**Fig. 7d**). The result indicated that the metal-protein direct contact is not necessarily required for this phenomenon.

Discussion

In this chapter, prior to the main finding, the phenomenon of electrostatic protein deposition was documented. There have been some previous experimental as well as molecular modeling studies concerning the organic molecule adsorption on gold surface in the presence of an external voltage (15-17). However, in spite of such earlier works, the adsorption mechanism behind has not been explicitly understood. So it should be emphasized here that the explicit understanding of the field-induced irreversible adsorption of protein is a remaining issue to be addressed in future.

Next, the finding of the voltage-regulated control of fluorescence protein emissions was described. Despite the history of fluorescence protein research of several decades, this simple phenomenon has not been documented to the best knowledge. Concerning organic small-molecule fluorophores, there have been some reports that may relate to our observations. Ruzgas et al. described potential-dependent changes in fluorescence intensity of Alexa 488 fluorophore covalently attached to the chemically modified gold electrode, in which a mechanism based on forester resonance energy transfer from the fluorophore to the metal was assumed. However, the signals reported there behaved differently from those in the present study, increasing for potentials both at more negative than -0.5 V and positive than +0.2 V. The similarity in the mechanism is hence not yet

obvious currently. Also, Kamat et al., demonstrated changes in the emission from pyrene fluorophore attached to gold nanoparticles by the degree of charges in the particles. Modulations in the rate of photo-induced electron transfer from pyrene to gold nanoparticle have been proposed as a mechanism there. But it is also not clear whether the phenomenon in this study share the same mechanism, considering that the time course of the responses in the present study seems much slower than expected from charge transfer mechanism and that the incorporation of intermediate layer did not much attenuate the modulations. It is expected that understanding the detailed mechanism may open various possibilities both in the life-science and applied physics fields. The points to be addressed toward this end would include analysis of photo-bleaching kinetics and fluorescence lifetime as a function of metal potential, the effects of metal types, the simultaneous electrochemistry, and the real-time measurements of the protein-metal distance.

References

1. O. Shimomura, F.H. Johnson, and Y. Saiga, J. Cell. Comp. Physiol. **59**, 223 (1962).
2. R.Y. Tsien, Annu. Rev. Biochem. **67**, 509 (1998).
3. E.A. Rodriguez, G.N. Tran, L.A. Gross, J.L. Crisp, X. Shu, J.Y. Lin, and R.Y. Tsien, Nat. Methods **13**, 763 (2016).
4. N. Tandeau de Marsac, Photosynth. Res. **76**, 193 (2003).
5. A. Kumagai, R. Ando, H. Miyatake, P. Greimel, T. Kobayashi, Y. Hirabayashi, T. Shimogori, and A. Miyawaki, Cell (2013).
6. A. Miyawaki, Annu. Rev. Biochem. **80**, 357 (2011).
7. A. Miyawaki, J. Llopis, R. Heim, J. Michael McCaffery, J.A. Adams, M. Ikura, and R.Y. Tsien, Nature (1997).
8. R. Ando, H. Hama, M. Yamamoto-Hino, H. Mizuno, and A. Miyawaki, Proc. Natl. Acad. Sci. (2002).
9. H. Tsutsui, S. Karasawa, H. Shimizu, N. Nukina, and A. Miyawaki, EMBO Rep. **6**, 233 (2005).
10. S. Habuchi, H. Tsutsui, A.B. Kochaniak, A. Miyawaki, and A.M. van Oijen, PLoS One **3**, e3944 (2008).
11. G.H. Patterson, Science **297**, 1873 (2002).

12. J. Lippincott-Schwartz and G.H. Patterson, Trends Cell Biol. **19**, 555 (2009).

13. R.A.G. Cinelli, V. Pellegrini, A. Ferrari, P. Faraci, R. Nifosì, M. Tyagi, M. Giacca, and F. Beltram, Appl. Phys. Lett. 79, 3353 (2001).

14. J.-W. Choi and M. Fujihira, Appl. Phys. Lett. 84, 2187 (2004).

15. J.R. Lakowicz, Anal. Biochem. **298**, 1 (2001).

16. H. Katayama, T. Kogure, N. Mizushima, T. Yoshimori, and A. Miyawaki, Chem. Biol. **18**, 1042 (2011).

17. T. Nagai, A. Sawano, E.S. Park, and A. Miyawaki, Proc. Natl. Acad. Sci. **98**, 3197 (2001).

18. Li, T. Ruzgas, and A.K. Gaigalas, Langmuir **15**, 6358 (1999).

19. P. V. Kamat, S. Barazzouk, and S. Hotchandani, Angew. Chemie Int. Ed. **41**, 2764 (2002).

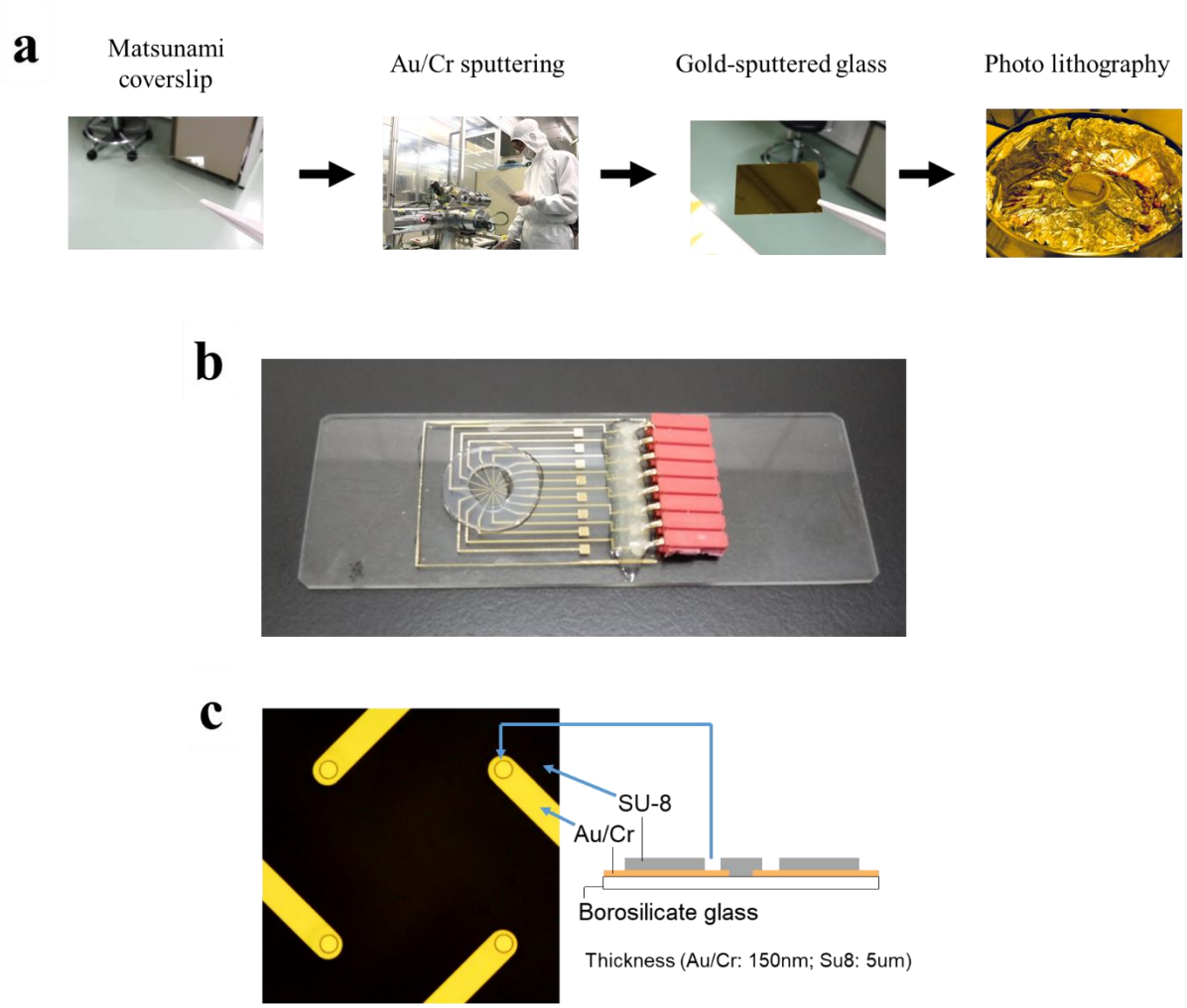

Figure 1. The microelectrode chambers for the experiments. (a) Fabrication process. (b) After mounting to the glass slide and connecting the terminals. (c) Micrograph showing 4 microelectrodes. The diameter of the electrode opening is ~ 50 μm in this example.

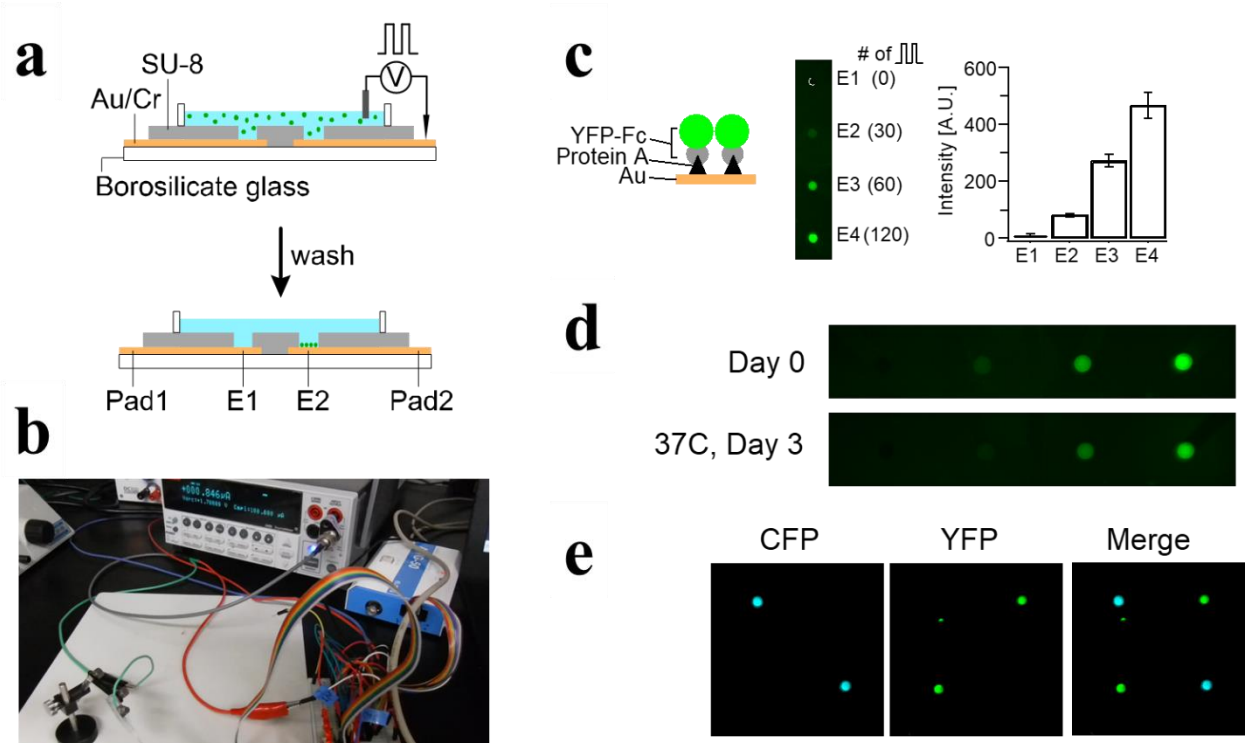

Figure 2. Electrostatic protein deposition onto gold microelectrodes.

(a) Schemes for protein electrodepositions onto the micro-patterned gold electrodes. (b) A picture showing the protein deposition apparatus. (c) An example of Protein-A electrodeposition using 100 ms square pulses of -1.7 V (vs. Ag/AgCl). Immobilization was detected by binding with YFP-Fc fusion protein. (*Note*: Fc is a protein domain which has binding affinity to Protein-A.) Amount of deposition was controllable by the number of pulses. (d) Electro-deposited Protein-A was detected immediately (*top*) or after 3 days' storage in phosphate buffered saline (pH 7.4) at 37°C (*bottom*). (e) Successive depositions of YFP and CFP in the two diagonal electrodes.

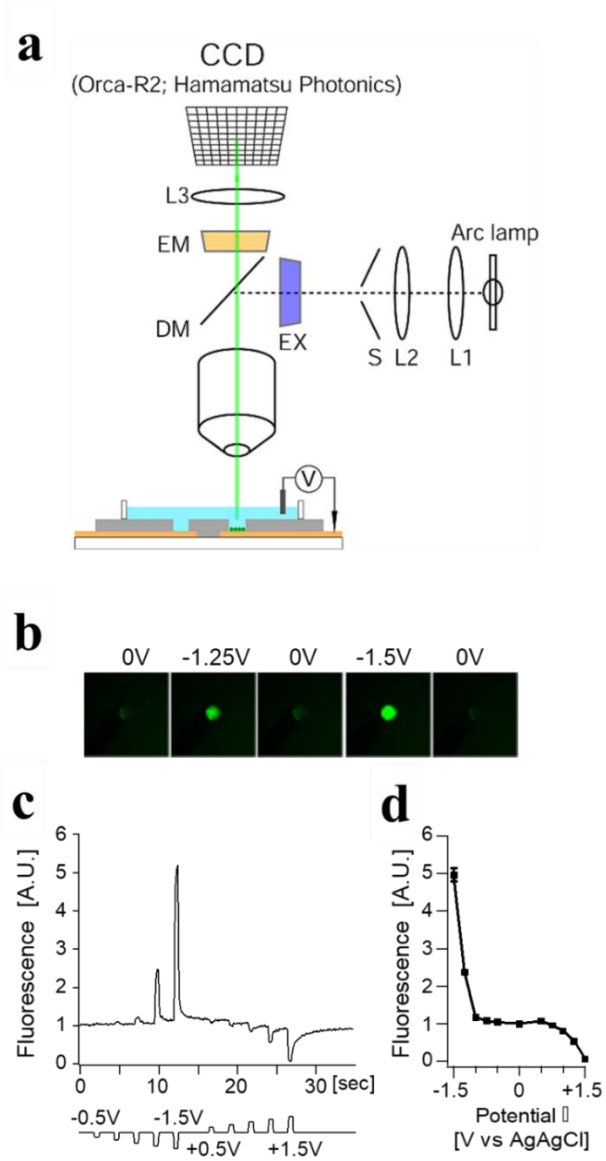

Figure 3. Voltage regulated fluorescence emission of fluorescence protein at the metal-solution interface. (a) Images show fluorescence from a YFP deposited electrode set at different potential as indicated (v.s. Ag/AgCl). (b) A time plot for the fluorescence intensity and the applied electrode potential. Fluorescence is normalized at time zero, 0 V. (c) A plot showing fluorescence versus electrode potential relationship (mean ± standard deviations of two independent datasets).

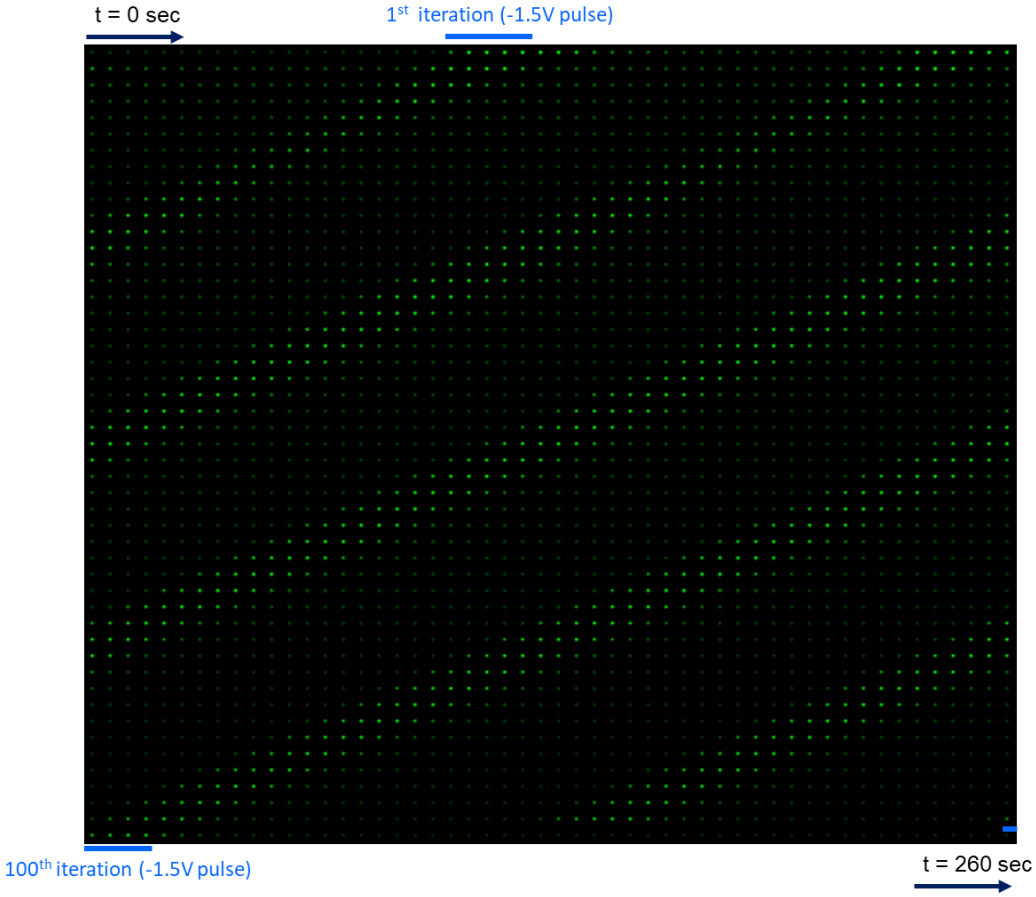

Figure 4. Repeatability of the voltage-regulated fluorescence modulation.

A montage of 2600 fluorescence images of the fluorescence protein immobilized electrode acquired for 260 sec at 10Hz. 100 iterations of negative voltage pulse application (-1.5V, 0.5sec) was performed during the recording.

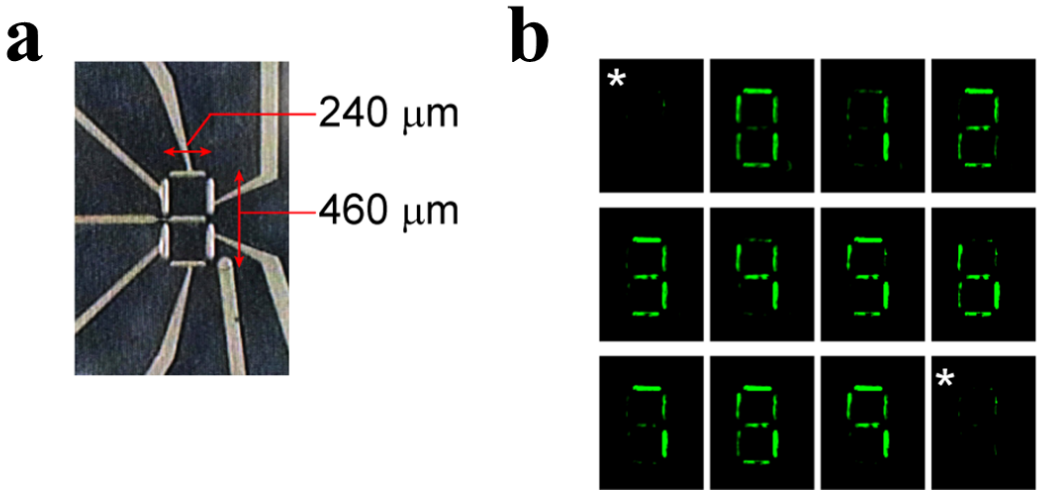

Figure 5. Protein based micro display. (a) A micrograph showing a micro-scale seven segment display based on fluorescence protein. (b) Operation of the display deposited with YFP. All the segments are turned off in the images with asterisk (*).

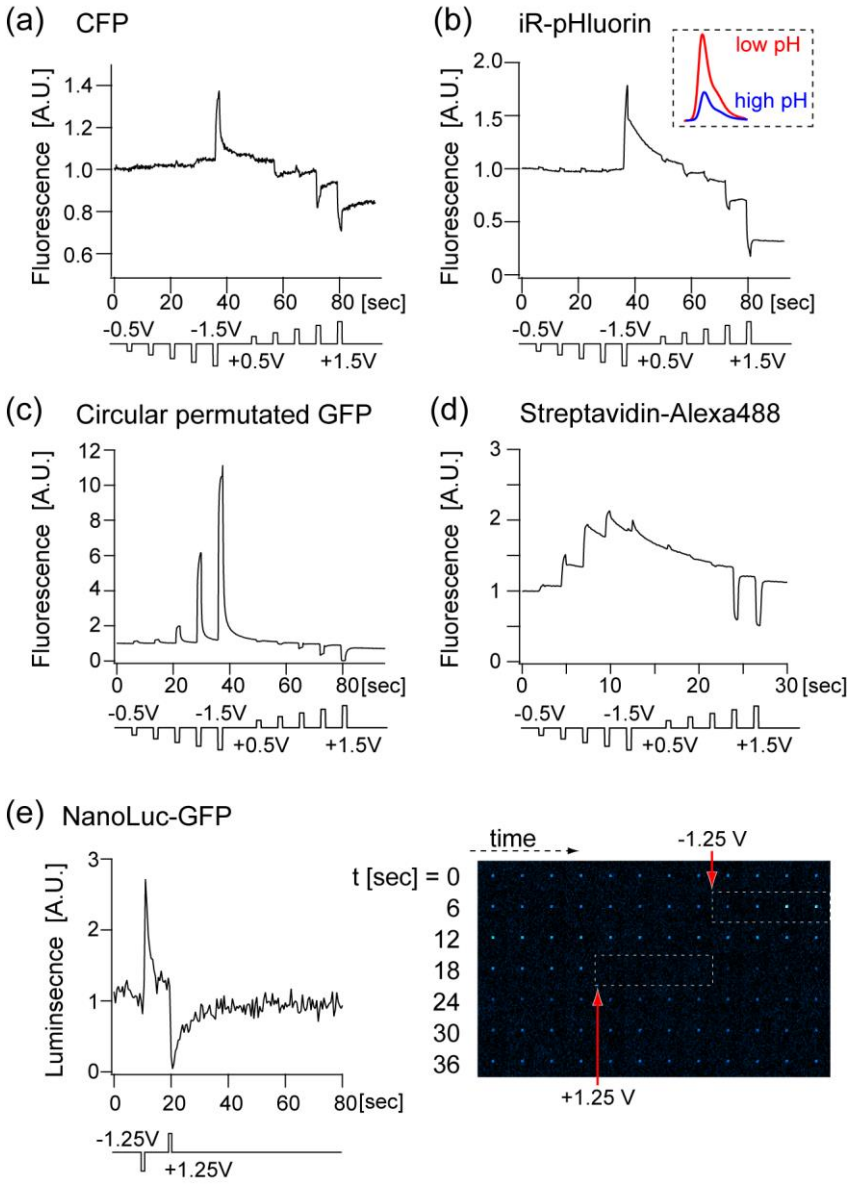

Figure 6. (a) Signal showing fluorescence modulation in CFP. (b) Signal from iR-pHluorin. The inset illustrates its pH-sensitivity which is reverse to that in YFP and CFP. (c) Signal from circular permuted GFP. (d) Signal from Streptavidin conjugated with Alexa 488. (e) Signal from NanoLuc-GFP fusion protein in the absence of excitation light, but in the presence of 10 μM furimazine (*left*). The time series of emission images in shown in the *right*. The voltage indicated was applied during the image frames shown by the dotted boxes.

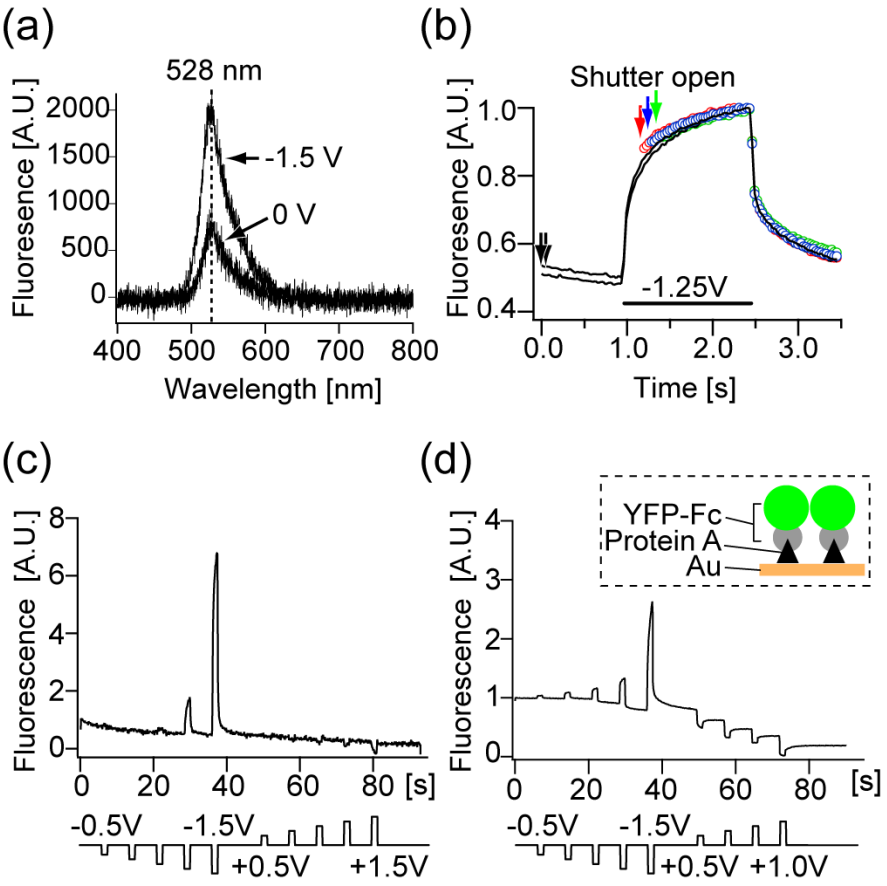

Figure 7. (a) Emission spectra from YFP at 0 or -1.5 V metal potential (v.s. Ag/AgCl). (b) The irradiations of excitation light were started before (*traces in black*) or after (*in colors*) the onset of -1.25 V pulse. Arrows indicate timings of shutter open. (c) Modulations of YFP emission at 20 mM MES pH 5.0, below the isoelectric point of YFP (5.7). (d) Modulation of fluorescence from YFP-Fc bound to the electro-deposited Protein-A as illustrated in inset.

Chapter 3: Mechanism

Voltage control of fluorescence protein emissions at the metal-solution interface

Chapter 3 Key Points

- The cathodic mechanism for the voltage regulated control of fluorescence protein emissions at the metal-solution interface was addressed by employing the characteristic properties of three different fluorescence proteins showing conventional pH-sensitivity, inverse pH-sensitivity, and green-to-red photo-convertibility.

- It was found that the interface-specific mode of protonation-deprotonation reactions underlies the cathodic effect, where the protonation state is directly coupled to hydrogen evolution at the interface rather than to the environmental acid-base equilibrium.

- This modulation mechanism opens a possibility that this interface effect may be utilized to enable spatially-resolved monitoring of hydrogen evolution reactions.

Introduction

In chapter 1, finding of an interface effect was described where emission from the fluorescence proteins immobilized at the metal-solution interface is modulated by changing the metal voltage to the solution. While the phenomenon has been implemented to develop a protein-based micro-display, the physicochemical mechanism behind the modulations has remained unresolved. In chapter 2, it was aimed to address mechanism underlying the interface effect.

In a protein, the titratable residues as well as the structural water molecules constitute a hydrogen-bond network through which the protons are transferred to or from the environmental bulk proton source, mediating the protonation-deprotonation reactions. Protonation-deprotonation equilibrium is also affected by the local hydrophobicity and electrostatic interactions. This often complicates the behavior of protonation in the titratable group facing inside of a protein at a given environmental pH (1-2). Concerning the fluoresces proteins (i.e., Aequorea green fluorescent protein and its homologs), there has been vast knowledge on their physicochemical properties in the bulk solution, as these have been of particular interest from the viewpoint of biomedical applications (3-6). Although this is a general scheme for a protein in the bulk solution, it is not well understood whether the interface effects could further alter the mode of protonation-

deprotonation. Here, through the elucidation of mechanism underlying the voltage regulated emission from the fluorescence protein at the metal-solution interface, existence of interface-specific mode of protonation-deprotonation reaction was found which may be utilized to enable spatially-resolved monitoring of hydrogen evolution reactions at the interface.

Materials and Methods

Details of the fabrication of a gold electrode chamber and the protein immobilizations were performed as described in chapter 1. Briefly, following the sputtering of a borosilicate glass substrate with chromium (30 nm) and gold (100 nm), the electrode lines and connecting pads were patterned with conventional photolithography. Then SU8-3005 (MicroChem, MA, USA) was patterned to form an insulation layer (5 μm) and the electrode openings (φ 40- 60 μm). For protein immobilizations, a protein of interest was prepared at 0.1 mg/ml in 20 mM 4-(2-hydroxyethyl)-1-piperazineethanesulfonic acid (HEPES; adjusted to pH 9.0) containing 1mM NaCl and 0.05% Triton-X surfactant. A source measurement unit (Keithley 2401, OH, USA) was used to electrostatically deposit protein by delivering brief positive voltage pulses (1.7 V, 100 ms) to the gold electrode to the Ag/AgCl electrode in the solution. The chamber was rinsed with pure water and filled

with the recording solution. Typically, the recording solution was 20mM HEPES (pH 7.4) containing 1mM NaCl but was modified in some measurements as noted.

Simultaneous electrochemistry and fluorescence microscopy

To enable simultaneous recording of current and fluorescence, an electrochemical analyzer (ALS 611E, CH Instruments, TX, USA) and a photomultiplier module (H5784-02, Hamamatsu Photonics, Japan) were operated in parallel. The protein-immobilized gold electrode, Ag/AgCl electrode, and a platinum wire ($\phi \sim 0.1$ mm) were used as the working, reference, and counter electrodes, respectively. We did not use an agar-bridge to couple the reference, since the whole chamber was as small as ~50 μl and so the solution leakage could result in a severe drift of polarization. The reference was immersed in the recording solution containing either 1- or 100-mM free chloride ions, where the calculated polarization of the reference was 0.4 or 0.28 V versus the saturated hydrogen electrode (SHE), respectively.

Results

Interface effect under an intense flow

First, the interface effect described in chapter 1 was re-examined under an intense flow. The aim was to test the assumption that if the negative bias could stimulate protein to temporally detach from the metal surface, the eventual removal of the metal-quenching effect should elicit fluorescence enhancement; then in the presence of the intense flow, protein would be washed out bias-dependently. The two glass-micropipettes were placed proximate to the electrode-well as an inlet and outlet **(Fig. 1a)**, through which the solution was circulated at the rate of 64 μl/s. The rate was significantly higher compared to the well volume of 6 ~ 14 pl. A yellow variant of green fluorescence protein, Venus was used for this test. The fluorescence modulation was repetitively observed without noticeable washout, confirming sufficient mechanical stability during the application of bias potential **(Fig. 1b)**.

Simultaneous electrochemical and fluorescence measurement

Next, it was asked whether the modulation is a field- or current-dependent process using a setup consisting of the fluorescence microscope and electrochemical analyzer (**Fig. 2a**). **Figure 2b** shows a representative time plot of fluorescence emission from Venus

and the current response to a cathodic potential scan in 20 mM HEPES containing 1mM NaCl. **Figure 2c** shows the current and fluorescent responses as a function of potential. From these results, it was evident that the cathodic effect of fluorescence modulation is tightly correlated with the electrode current.

Origin of the current associated with the fluorescence modulation

Aiming to understand the origin of the current, the current in the bare (i.e., gold only) and the protein-deposited electrodes were compared. In both cases, the exponential evolution of current was observed at ~ -1.2 V or more negative potential (**Fig. 3a;** arrowheads), showing the cathodic hydrogen evolution reaction (HER) at the interface. In the bare electrode, a characteristic shoulder component of the current which proceeds the exponential component was observed (**Fig. 3a;** arrows). Since the shoulder component was observed only in the presence of HEPES (**Fig. 3b)**, it was reasoned that the shoulder current reflects the proton release from HEPES and the subsequent supply onto the metal surface for reduction. The elimination of shoulder current by protein immobilization (**Fig. 3a**) suggested that that the proton supply from 20mM HEPES tends to be constrained by the existence of protein at the interface. However, such barrier effect by protein was overwhelmed when HEPES concentration was raised to 50

mM; the shoulder component became evident even in the presence of protein at the interface (**Fig. 3c).** Importantly, we then found that whereas 50 mM HEPES enhanced the electrode current, it attenuated the fluorescence modulation (**Fig. 3d**). Because we also confirmed that the high salt recording solution (100 mM NaCl solution; Deby length = 0.96 nm) does not attenuate the modulation (data not shown), the decline of fluorescence response by 50 mM HEPES was not due to the increased ionic strength but was brought by its nature as a proton buffer.

Hypothesis: protonation-deprotonation reaction drives the fluorescence modulation

To sum up the knowledge so far, the fluorescence modulation was correlated to the hydrogen reduction at the metal surface (**Fig. 2**) and was attenuated by the high concentration proton buffer (**Fig. 3**). These results straightforwardly suggested an involvement of the protonation-deprotonation reactions. All the known fluorescence proteins are sensitive to protonation-deprotonation reactions. Regarding the fluorescence proteins in which the chromophore possesses the phenolic hydroxyl group, including Venus (7-8), the protonation state of the hydroxyl group is the most critical factor for its fluorescence. The group exists either in the protonated or deprotonated state. In the case

of Venus, only the latter state is fluorescent with the absorption and emission peaks at 515 and 528 nm, respectively (**Fig. 4**). So, it was hypothesized that the negative bias directs the equilibrium toward the direction of deprotonation.

Verification of the involvement of protonation-deprotonation reaction based on the green-to-red photoconversion in KikGR

To verify the hypothesis from a different point of view, the green-to-red photoconversion exhibited by a certain type of fluorescence protein was focused. KikGR is one such protein. KikGR is originally a green-emitting (emission peak at 517 nm) after its protein synthesis and folding. Its green chromophore possesses the phenolic hydroxyl group which exists either in the protonated (absorption peak at 390 nm) and deprotonated state (507 nm). Notably, the photoexcitation of the protonated state leads to the irreversible conversion into a red chromophore through β-elimination and subsequent extension of the π-conjugation system, whereas the photoexcitation of the deprotonated form does not (9-10) (**Fig. 4)**. The hypothesis that the chromophore deprotonation is driven by the negative potential bias therefore predicted that the negative bias should inhibit the green-to-red photoconversion. To test this, '*J, a, i, s, t*' shaped micro-electrodes was fabricated and immobilized with green KikGR protein (**Fig. 5a**). As was seen on Venus, the green

fluorescence of KikGR at the excitation of blue light exhibited enhancement upon application of -1.5 V bias potential. Initially, red fluorescence at the excitation of green light was undetectable. Then UV light (352-402 nm; 1.8 mW/cm^2) was irradiated for 20 seconds to induce green-to-red photo-conversion. During the irradiation, -1.5V bias potential was applied to the electrode '*i*', whereas the other electrodes were left open-circuited (**Fig. 5b**). After the irradiation, all the electrodes were open-circuited and were subject to fluorescence observation. Then, as expected from the hypothesis, the electrode '*i*' remained green after irradiation whereas the others had undergone significant green-to-red photoconversion (**Fig. 5c**). Because green-to-red photoconversion is a photochemical process that is only dependent on the photoexcitation but not on the emission, the result provided direct evidence that adsorption is affected by the negative bias. In this way, the photoconversion experiments verified that the protonation-deprotonation equilibrium of interfacial protein is regulated by potential at the metal.

Existence of interface specific mode of protonation-deprotonation

It was then addressed how the negative bias drives proton deprotonation. Although one simplest view could be the pH elevation due to the proceeding of proton reductions at the cathode, existing pilot experiments did not support that view as mentioned in chapter 1.

iR-phuruolin exhibiting the *inverse* pH sensitivity was again used to address this issue more explicitly. iR-phuruolin is a mutant of ratiometric pHuluorin (11) which carries three additional mutations and exhibits improved brightness (11-12). Its chromophore possesses the phenolic hydroxyl group and has bimodal excitation peaks at 390 and 481 nm which correspond to the excitation of the protonated and deprotonated states, respectively. Importantly, the protonation equilibrium of the hydroxyl group of iR-pHluorin responds to external acidity unconventionally; the protonated state predominates at high pH and vice versa for the deprotonated state (**Fig. 4**). In short, at blue light excitation, Venus and iR-pHluorin get brighter and dimmer for higher external pH, respectively, vice versa for lower pH. At UV light excitation, iR-pHluorin gets brighter for higher pH, vice versa for lower pH. While these are knowledge only known from the previous solution studies, it was validated that Venus and iR-pHluorin immobilized at the metal-solution interface still retain the same conventional and inverse pH-sensitivity, respectively (**Fig. 6a**). Based on this knowledge, the key to this experiment was to examine the direction of shift in the protonation-deprotonation equilibrium. **Fig. 6b** and **6c** show iR-pHluorin responses at the excitation of blue (497/16 nm) and UV (377/50 nm) light, respectively, to the cathodic potential scan at 0.1 V/s. The recording solution did not contain HEPES so that signals derived from local pH change could be

sensitively detected. Despite such experimental condition, the direction of the major response at blue light excitation (**Fig. 6b**, t=14 sec) was unchanged from that of Venus (**Fig 2b, c**), and fluorescence at UV light excitation did respond as fluorescence decrease (**Fig. 6c,** t=14 sec). These results revealed that even in iR-pHluorin with the inverse pH-sensitivity, chromophore deprotonation was proceeded by the negative bias potential, which is not explained by the local alkalization but by the direct effect of interfacial hydrogen evolution reaction.

Mechanism for the cathodic fluorescence modulation

It was thus concluded that the interface-specific mode of protonation-deprotonation reactions underlies the cathodic control of fluorescence protein emission. **Figure 7** illustrates the mechanism. In solution, the protonation pattern of the titratable groups is determined through the acid-base equilibrium of the bulk proton source such as water and buffers (**Fig. 7a**; black arrows). At the metal-solution interface, the application of negative bias potential drives transfers of protons from the environmental proton source for the adsorption and reduction on the metal surface (**Fig. 7b, c**; green arrows). As was seen in **Figure 3a-c**, such supply tends to be restricted by the presence of protein at the interface**.** In a protein immobilized at the interface, the interface-specific mode of direct interactions

between the intra-protein groups and the metal surface is also established (**Fig.7b**; red arrows), which is distinct from the detour paths consisting of the protein-environment and environment-metal interactions (**Fig. 7b**; green + black arrows). Thus, the protonation-deprotonation of a given group, including the phenolic hydroxyl group of the chromophore, is contributed both by the environment and metal-surface conditions (**Fig. 7b**; black, red arrows). Upon the application of negative bias and eventual proceeding of HER steps (i.e., the Volmer and Heyrovsky steps) on the metal surface, protons could be supplied both from the environmental proton source (**Fig. 7**; green arrows) and from the intra-protein groups (**Fig. 7**; red arrows). While the former process promotes alkalization of the local environment, which tends to drive deprotonation of the phenolic hydroxyl group in Venus chromophore but protonation in iR-pHluorin chromophore, the present results that the deprotonation did proceed in iR-pHluorin chromophore indicated that the protein-metal direct interactions are dominant, serving as the major mechanism for the cathodic fluorescence modulation (**Fig. 7;** red arrows). Moreover, these multiple interactions compete, which explains the increased electrode current as well as the attenuated fluorescence modulation caused by the increased concentration of the proton buffer (**Fig. 3d**).

Discussion

In this chapter, it was revealed that interface-specific mode of protonation-deprotonation reaction, which is driven through the proceeding of interfacial hydrogen evolution reaction, underlies the voltage regulated modulation of fluorescence protein emission at the metal-solution interface. At this stage, it is yet difficult to obtain a more detailed structural basis for the interface-specific metal-protein interactions. One important point would be to understand why the interface-specific mode of protonation-deprotonation reactions (**Fig. 7c**; green arrow) has the dominant effect on the protein protonation at the negatively-biased interface. One conjecture is that the dominance may be caused by the charge neutralization condition which should not be necessarily held at the interface. Although the modulation mechanism was elucidated by focusing on the phenolic hydroxyl group in the three fluorescence proteins. However, it should be emphasized that the hydroxyl group is a prerequisite for the effect. That is because the properties of the chromophore are also sensitive to the protonation patterns of the surrounding titratable groups. For example, whereas the chromophore of a cyan-emitting fluorescence protein does not possess the phenolic hydroxyl group, it has been suggested that its isomeric configuration is dependent on the protonation of the surrounding residues including the 148^{th} residue (13-15) (**Fig. 4)**. It is therefore reasonable that CFP exhibited a similar

catholic modulation at the interface.

The interface effect on fluorescence protein was previously implemented as a protein micro-display previously, and in this study, to perform an irreversible photo-recording of input signal pattern using the photo-convertible fluorescence proteins (**Fig. 5a-c**). By combining with the single-molecule detection technique (16), these will be operated in much higher spatial density. Another interesting subject should be the monitoring of HER. Improvements in the electro-catalytic efficiency of HER is in high demand for efficient energy conversions and the establishment of a sustainable society[17]. While the current-potential relationship (i.e., Tafel plot) provides an accurate criterion for the efficacy (17-18), it does not well report on the spatial inhomogeneity of catalysis over the cathode. Fluorescence protein at the interface may serve as a unique optical indicator of HER, which should help to develop innovative catalytic materials as well as the electrode microstructures.

References

1) F. Garczarek and K. Gerwert, Nature 439, 109 (2006).

2) G.M. Ullmann and E.W. Knapp, Eur. Biophys. J. 28, 533 (1999).

3) R.Y. Tsien, Annu. Rev. Biochem. 67, 509 (1998).

4) N.C. Shaner, P.A. Steinbach, and R.Y. Tsien, Nat. Methods 2, 905 (2005).

5) A. Miyawaki, Annu. Rev. Biochem. 80, 357 (2011).

6) A. Miyawaki, J. Llopis, R. Heim, J. Michael McCaffery, J.A. Adams, M. Ikura, and R.Y. Tsien, Nature (1997).

7) T.D. Farha, K. Hama, M. Imayasu, Y. Hiratsuka, A. Miyawaki, and H. Tsutsui, Appl. Phys. Express 12, 067001 (2019)

8) T. Nagai, K. Ibata, E.S. Park, M. Kubota, K. Mikoshiba, and A. Miyawaki, Nat. Biotechnol. 20, 87 (2002).

9) H. Tsutsui, S. Karasawa, H. Shimizu, N. Nukina, and A. Miyawaki, EMBO Rep. 6, 233 (2005).

10) H. Tsutsui, H. Shimizu, H. Mizuno, N. Nukina, T. Furuta, and A. Miyawaki, Chem. Biol. 16, 1140 (2009).

11) G. Miesenböck, D.A. De Angelis, and J.E. Rothman, Nature 394, 192 (1998).

12) H. Katayama, T. Kogure, N. Mizushima, T. Yoshimori, and A. Miyawaki, Chem. Biol.

18, 1042 (2011).

13) G.D. Malo, L.J. Pouwels, M. Wang, A. Weichsel, W.R. Montfort, M.A. Rizzo, D.W. Piston, and R.M. Wachter, Biochemistry 46, 9865 (2007).

14) G. Vallverdu, I. Demachy, F. Mérola, H. Pasquier, J. Ridard, and B. Lévy, Proteins Struct. Funct. Bioinforma. 78, 1040 (2010).

15) A. Fredj, H. Pasquier, I. Demachy, G. Jonasson, B. Levy, V. Derrien, Y. Bousmah, G. Manoussaris, F. Wien, J. Ridard, M. Erard, and F. Merola, PLoS One 7, e49149 (2012).

16) S. Shashkova and M.C. Leake, Biosci. Rep. 37, 20170031 (2017).

17) N. Dubouis and A. Grimaud, Chem. Sci. 10, 9165 (2019).

18) T. Shinagawa, A.T. Garcia-Esparza, and K. Takanabe, Sci. Rep. 5, 1 (2015).

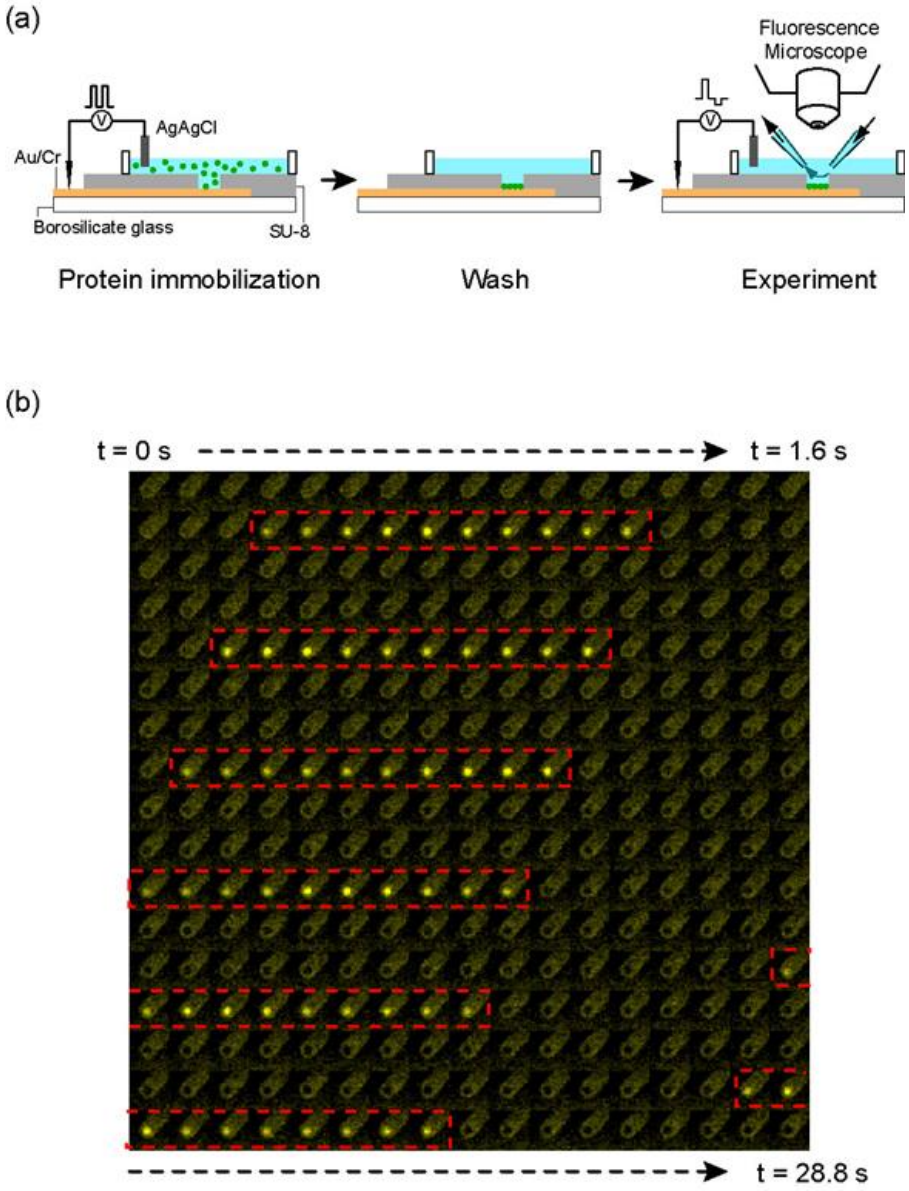

Figure 1. Observation of the interface effect under an intense flow of recording solution. (a) A scheme for the experiment. (b) A montage showing the fluorescence modulation. A negative bias of -1.5 V was applied during the frames indicated by red.

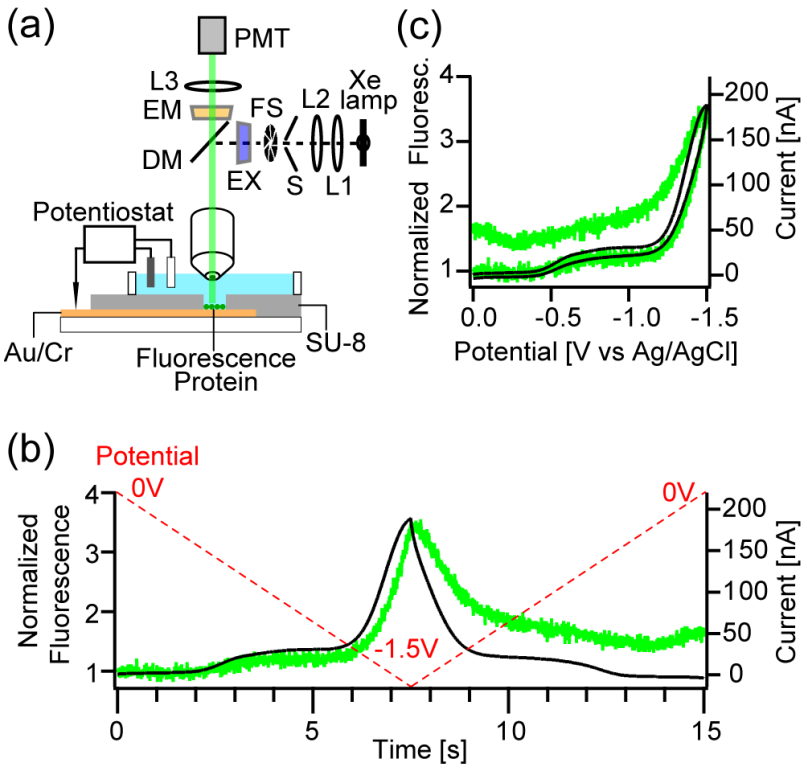

Figure 2. The simultaneous fluorescence and current measurements.

(a) A scheme of the setup. L1-L3: lens for collection and projection; S: shutter, Em: emission filter, Dm: dichroic mirror, Ex: excitation filter; FS: field stop to restrict the area of photoexcitation. (b) A representative fluorescence (in green) and current (in black) response versus time. Applied potential is over-plotted in red. (c) A plot of the fluorescence and current response versus the electrode potential.

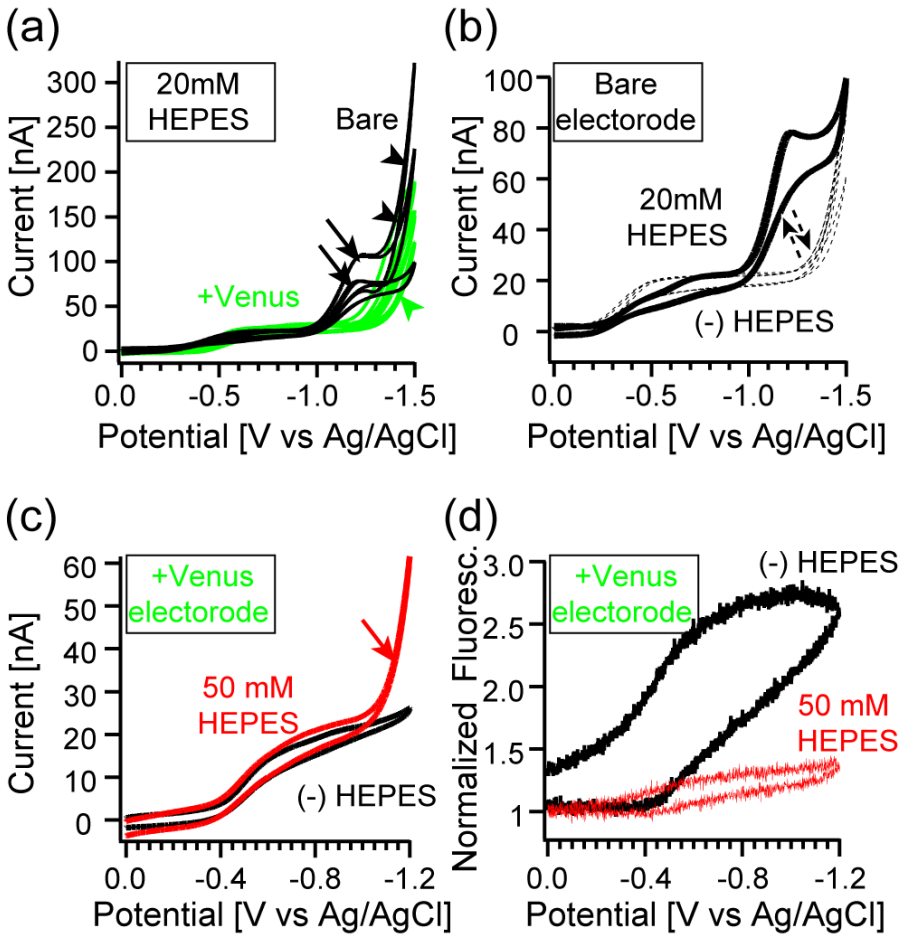

Figure 3. Analysis of the factors affecting the electrode current.

(a) The current responses as a function of potential in the bare (*in black*) and protein deposited (*in green*) electrodes. Recording solution was 20 mM HEPES, 1mM NaCl. Data from three electrodes (φ~60 μm) is over-plotted. (b) Current responses of a bare electrode in the absence of HEPES (i.e. 1mM NaCl; *dotted*), after addition of 20mM HEPES (*plain*), and after washout of HEPES (*dotted*). (c) Current responses of a protein-deposited electrode in the presence (*in red*) or absence (*in black*) of 50 mM HEPES. The arrow indicates HEPES dependent shoulder component. Note that scale for *x*-axis is 0 ~ -1.2V. (d) Fluorescence signal in the presence (*in red*) or absence (*in black*) of 50 mM HEPES.

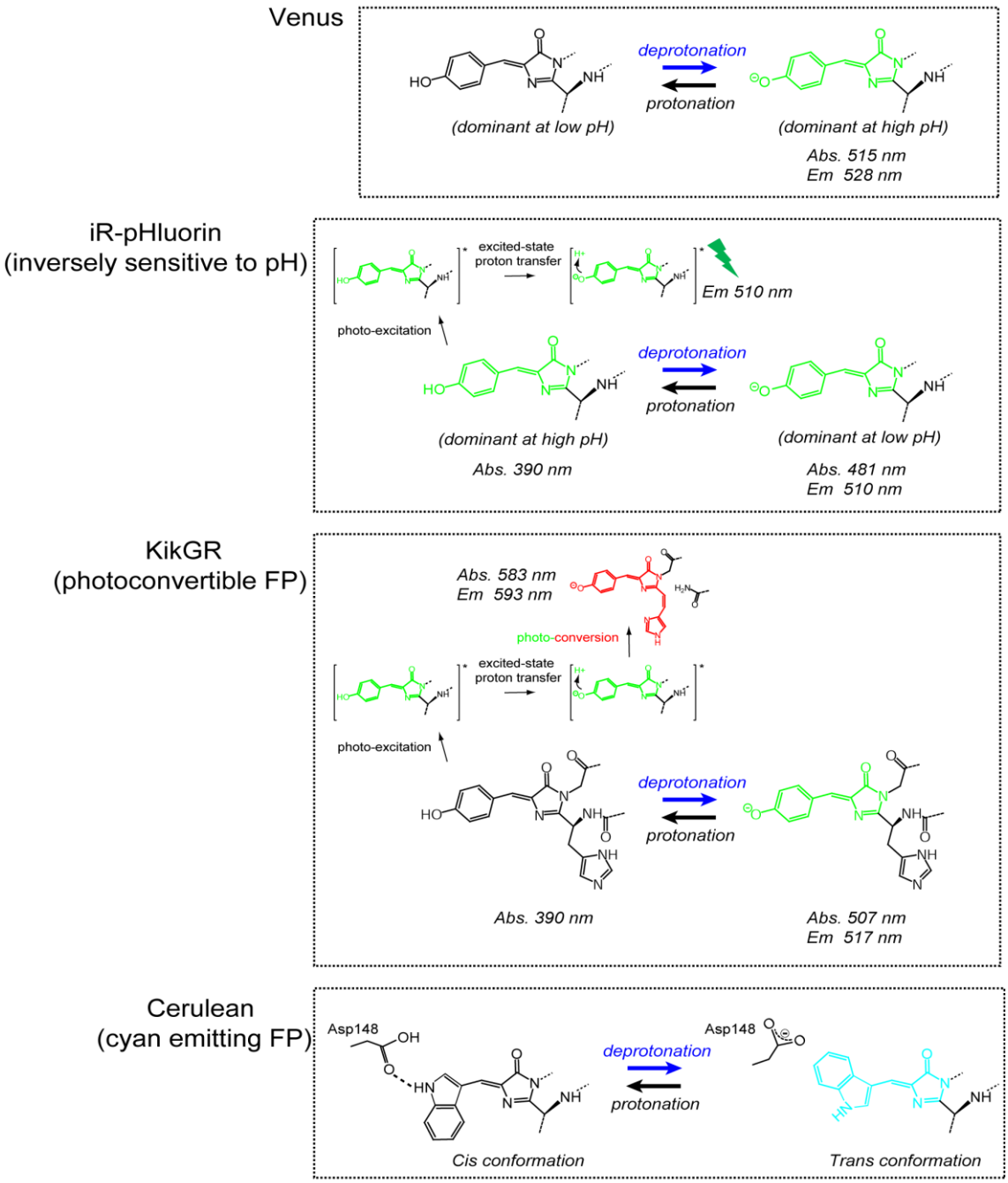

Figure 4. A scheme summarizing properties of the chromophore in Venus, iR-pHluorin, KikGR, and Cerulean CFP. The bracket with an asterisk (*) indicates chromophore in the excited state. The light wavelengths for the peak of absorption (Abs) and steady-state fluorescence emission (Em) are shown.

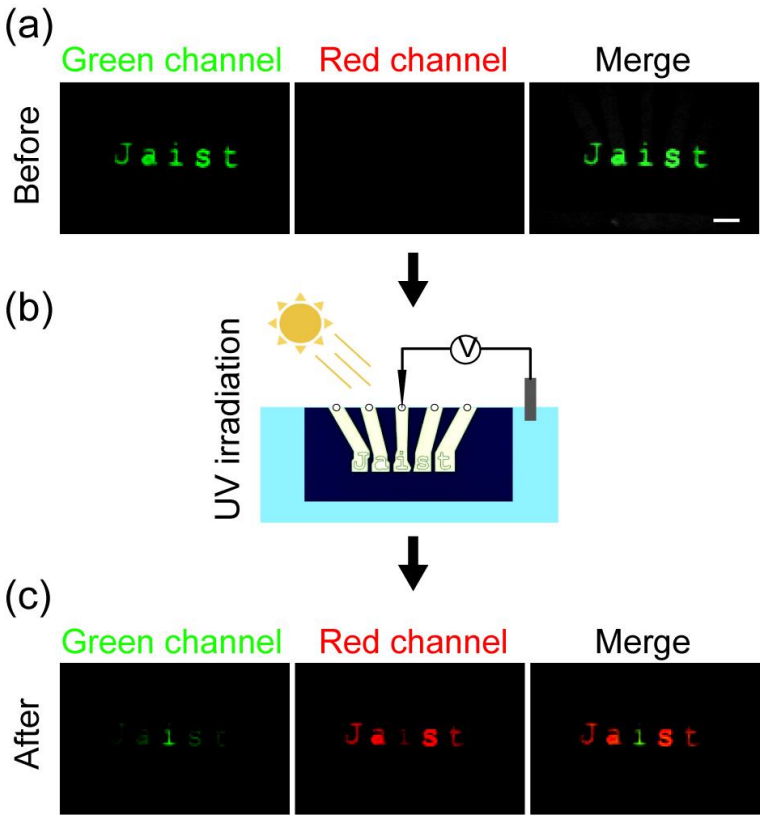

Figure 5. An optical recording of input signal pattern using green-to-red photoconversion. (a) Letter-shaped microelectrodes immobilized with unconverted (green) KikGR protein. The filters and mirrors used were Ex: 470/20, Dm: 485, Em: 517.5/45 nm for the green channel; Ex: 535/50, Dm: 565, Em: 610/75 nm for the red channel. The experimental solution was 1mM NaCl, 20 mM HEPES, pH 7.4. Bar = 100 μm. (b) During the UV irradiation, a bias potential of -1.2 V was applied to electrode 'i' to unselect for photoconversion. (c) Fluorescence image after the UV irradiation.

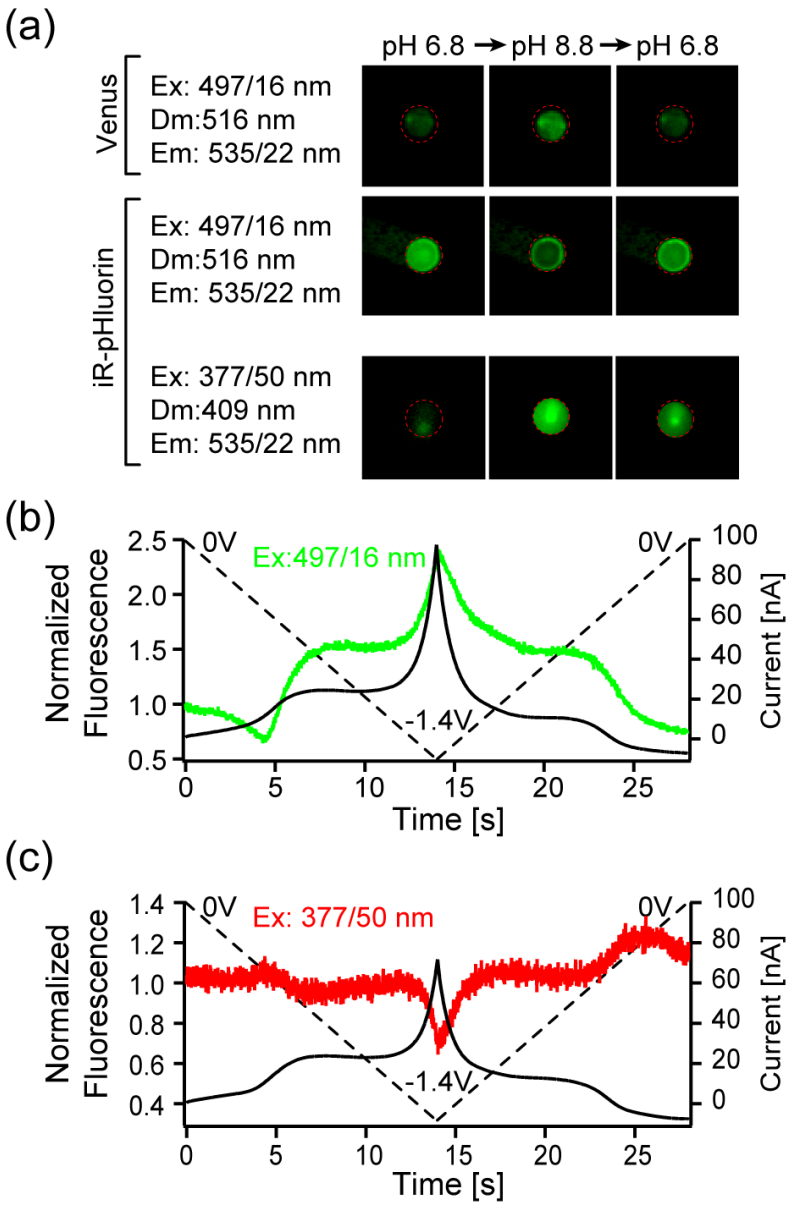

Figure 6. Cathodic effect on iR-pHluorin.

(a) Images showing fluorescence from electrode immobilized with Venus or iR-pHluorin at pH adjusted to 6.8 or 8.8 with 50 mM Tris buffer. The optical filters used are indicated. The excitation at 497 and 377 nm respectively correspond to the blue and UV light excitation mentioned in the text. (b, c) Responses of iR-pHluorin fluorescence at the excitation with blue light (*b, in green*) or UV light (*c, in red*). The applied potential is over-plotted in a dotted line.

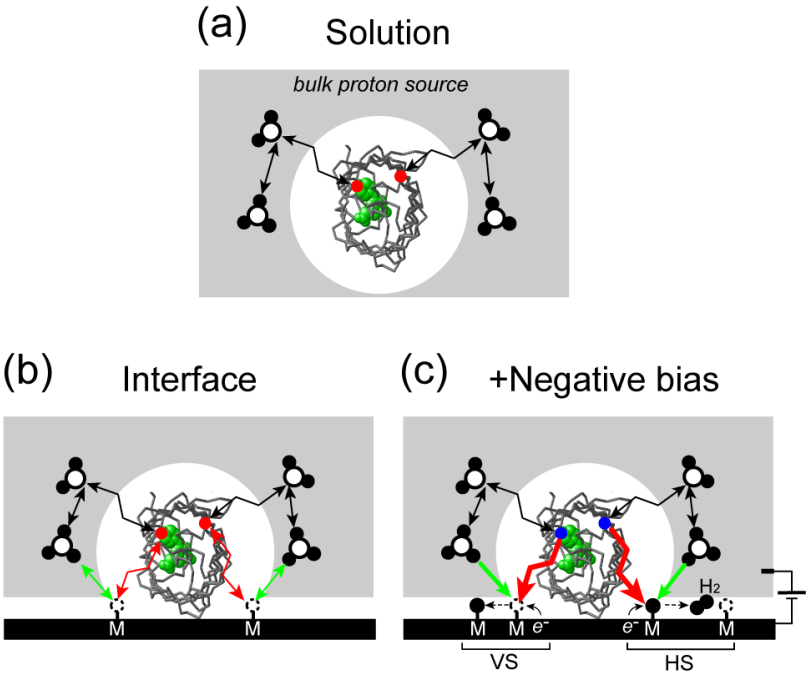

Figure 7. Mechanism for the cathodic modulation of fluorescence protein emission. (a) Protein in solution. The two red circles in the fluorescence protein model symbolically indicate intra-protein titratable groups. The black arrows: proton-transfer pathways between the groups and the bulk proton source. (b) Protein at the metal-solution interface. Metal atom (M) is also a proton acceptor. The green arrows: proton transfer paths between the metal and environmental proton source. The red arrows: the interface-specific paths allowing direct interaction between the metal and intra-protein groups. (c) In the presence of negative bias, hydrogen evolution reaction drives transfers of proton not only from the bulk source (green arrows) but also from the intra-protein groups (red arrows), affecting fluorescence. VS and HS: Volmer and Heyrovsky step of the hydrogen evolution reaction. Note that proteins are considered to be randomly oriented in the current experiment.

Chapter 4: Application

HER imaging based on the voltage control of fluorescence protein emissions at the metal-solution interface

Chapter 4 Key Points

- The possibility of utilizing the interface effect described in **Chapter 1** as an optical indicator of HER (hydrogen evolution reaction) was addressed.

- The simultaneous electrochemistry and optical imaging experiments showed high coloration between the fluorescence and HER activity both in the spatial and temporal aspects.

- The optical signal is contributed both by the direct HER driven deprotonation effect as well as the minor effect driven through the local acid-base equilibrium change.

- Optical imaging of the electrode with a catalysis pattern clearly visualized the pattern-specific activation pattern of HER. Especially, the propagating nature of HER was found for which the detailed mechanism remains to be solved in future.

Introduction

The fluorescence protein technologies employing the family of *Aequorea victoria* green fluorescent protein (GFP) and the other GFP-like proteins have revolutionized modern cell biology by allowing the genetic synthesis of bright fluorophores inside the living cells. These techniques take advantages of their rich physico-chemistry, including the various hue palettes, resonance energy transfers between a pair of fluorophores as well as the dynamic photo-switching behaviors. Because of the cell biological purpose, these fascinating and useful physico-chemical properties and behaviors of fluorescence proteins have been mostly investigated in the bulk solution whereas the physico-chemistry at the surface or interface have been less focused. In chapter 1, the interface effect was described in which fluorescence protein immobilized at the gold-solution interface exhibits robust voltage dependent modulation of fluorescence emission. In chapter 2, it was revealed that the modulation induced by the negative bias voltage is driven through the interface-specific mode of protonation-deprotonation reactions. At the interface, the protein protonation is directly coupled to the occurrence of hydrogen evolution reaction (HER) rather than via the local pH environment. Given the keen dependence of fluorescence protein emission on its protonation state, this finding opened a possibility of utilizing fluorescence protein as an indicator of hydrogen evolution

reaction at the metal-solution interface.

HER is one of the two half reactions in the electrochemical water-splitting. Attaining the optimal environment of HER is one of today's pressing issues toward the efficient production of molecular hydrogen, the clean-burning energy-dense fuel (1-4). Although the Spatio-temporal visualization of HER could provide essential information in understanding and achieving optimal condition for HER, few existing techniques allow scanning-less real-time imaging (5, 6). This chapter aims to address the possibility and limitations of utilizing fluorescence protein emission at the metal-solution interface as an optical indicator of HER.

Materials and Methods

Microelectrode chambers

An ion beam sputtering system (EIS-220, Elionix, Tokyo) was used to sputter a borosilicate glass substrate (22 × 32 mm) with chromium and gold to the thickness of 30 and 200 nm, respectively. After photolithographic patterning of the electrodes, a mask layer of Su-8 3005 (MicroChem, MA, USA) was formed with the open windows for catalysis deposition. Following sputtering of platinum/palladium (Hitachi E-1030), the mask was removed by piranha solution treatment. This process was omitted for the experiments not using a Pt/Pd island. Finally, a new layer of Su-8 3005 was pattered to

form an insulator, microelectrode chambers, and the connection pads. After hard baking of the whole device (200 °C; 10 min), a silicone elastomer washer (id = 6 mm, o.d. = 13 mm) was attached using a poly-dimethylsiloxane elastomer to configure a solution chamber. The chamber was plasma-cleaned before use (PDC-32G, Harrick Plasma, N.Y., USA).

Protein preparation and deposition:

Protein expression in Escherichia coli (strain: JM109DE3) and purification by Ni2+ affinity chromatography were performed as described in chapter 1. For protein deposition, after placing 70 ul protein solution (~100 ng/ml in 20 mM HEPES (pH 9.0) buffer, 1 mM NaCl, 0.05% Triton-X) into the chamber, external voltage pulses (amplitude 1.6 V; duration 100ms; 100 pulses) were applied to the microelectrodes with respect to the Ag/AgCl electrode immersed in the solution by using a source measurement unit (Keithley 2401, USA). The chamber was rinsed with pure water and filled with the recording solution consisting of 20 mM HEPES (pH 7.4) and 1 mM NaCl.

Measurements and analysis

The measurement setup consisted of an electrochemical analyzer (ALS 611E, CH Instruments, TX, USA), a CMOS-camera (C11440, Hamamatsu Photonics, Japan), and

an upright fluorescence microscope (Olympus BX51WE, Japan) equipped with a water immersion (60x) objective and a stable Xenon lamp. The reference Ag/AgCl electrode was directly immersed in the recording solution. The calculated polarization of the reference was 0.4 versus the saturated hydrogen electrode. The electrochemical analyzer and c-MOS camera were synchronized with an external trigger from a pulse generator (AWG-50, Elmos, Japan). Images were analyzed using image J and a homebuilt program of IDL (Research Systems).

Results

Figure 1 illustrates the concept of HER imaging. At a resting condition, the chromophore's phenolic hydroxyl group exists at the protonation/deprotonation equilibrium (**Fig. 1a**). Upon activation of HER, the protein at the interface acts as a proton donor to the active sites of metal and metal-hydrogen pairs (**Fig. 1b-d**), which is defined as a direct deprotonation effect of HER. During activation of HER, the hydronium ion and the buffer in the solution also donate protons, which induces local alkalization and hence affects the protonation state of fluorescence protein. We define such local-pH mediated influence as a secondary effect. Aiming to discriminate the direct and secondary effects, we used two different fluorescence proteins, Venus and dKeima, in this study.

Venus is a yellow fluorescence emitting variant of GFP, in which the deprotonated chromophore emits bright fluorescence peaking at 528 nm upon blue light excitation whereas the protonated state is almost non-fluorescent. dKeima is a coral-derived red fluorescence protein in which the protonated and deprotonated states have excitation peaks at 440 nm and 586 nm, respectively, and the both emit at 620 nm (7). A key contrast between these two proteins is in the way of their response to external pH; the protonated state predominates at low and high pH in Venus and in dKeima, respectively, and vice versa for the deprotonated state (7, 8). Although such properties have been known in the solution environment, it was verified that the proteins immobilized at the metal-solution interface show the same trend (**Fig. 2**).

HER-induced optical signals: temporal correlation

First, we examined the temporal correlation between HER and the fluorescence response under the different potential scan rates. Following protein immobilization onto a ϕ50 μm gold microelectrode, current and fluorescence signals elicited by the potential sweep from 0 to -1.7 [V vs Ag/AgCl] were simultaneously measured (**Fig. 3a**). Four different scan rates: 0.1, 0.2, 0.5, and 1 [V/sec] were tested. Blue (489-505 nm) and green light (510-560 nm) was used for the excitation of deprotonated forms of Venus and dKeima,

respectively. As an overall trend, the current and fluorescence signals were temporally correlated in all the scan rates both in Venus (**Fig. 3b**) and dKeima (**Fig. 3c**). The important point was that the directions of the major optical signals were identical (i.e. fluorescence increase) for these two proteins irrespective of the opposite sensitivities to external pH. This observation reflected that the protonation state around at the large negative voltage (-1.5~-1.7 V) is driven though the direct deprotonation effect rather than through the local acid-base equilibrium, or the secondary effect. For the fluorescence responses in Venus, full widths at half maximum (FWHM) for the scan rate of 0.1, 0.2, 0.5, and 1 [V/sec] were: 3.3 ± 0.3 (average ± s.d; n=4), 1.7± 0.1(n=2), 0.76 ± 0.05 (n=2), and 0.38 ± 0.01 (n=2) [sec], respectively. FWHMs of dKeima signals at these scan rates were: 1.8 ± 0.1 (n=4), 1.0 ± 0.1(n=3), 0.43 ± 0.05 (n=3), and 0.23 ± 0.04 (n=3) [sec], respectively. The differences of FWHM at each scan rate were statically significant (Welch's t test, $p<0.05$). Thus, dKeima generally produced shorter responses than Venus. It was reasoned that the difference is due to the secondary effect. Since the buffer molecule and hydronium ion also act as proton acceptor upon the activation of HER, HER causes local pH elevation, thus facilitates chromophore deprotonation in Venus and protonation and dKeima, respectively. In dKeima responses, slight fluorescence decreases were mostly evident at the low negative voltage range (>~-1.4V; **Fig. 3c**), showing that

the local pH effect is dominant in this region. In this way, the direct effect of HER-driven deprotonation and the indirect effect of local pH elevation affect Venus signal in the same direction whereas affect dKeima signal in the opposite direction. **Figure 3d** shows delay of optical signals from the electrode currents quantified from the cross-correlation analysis. Owing to the acute fluorescence response, dKeima exhibits substantially shorter delay than Venus.

HER-induced optical signals: spatial correlation

Next, aiming to study spatial correlations between HER and the fluorescence signals, we fabricated 'coffee-bean' shaped split microelectrodes. A gap of 5~8 um in width was formed to constitute a pair of electrically-independent semicircular electrodes. After depositing proteins onto both electrodes, fluorescence imaging was performed while applying bias voltage to either one of the electrodes to activate HER and the other remained open-circuited, which we refer the active and the resting electrode, respectively. In the experiment using Venus, whereas the robust increase of fluorescence was observed from the active electrode (**Fig. 4a, b**), slight but non-negligible increase of fluorescence was also detectable in the resting electrode especially at the region near the gap (**Fig. 4c, d**). We assumed that that this minor intensity changes at the resting electrode could be

due to the increased light scattering of fluorescence at the active electrode nearby, and/or to the local pH gradient formed by the solute diffusion. To discriminate these possibilities, dKeima signals in response to the potential scan were examined. In the active electrode, as was observed in the single electrode experiments (**Fig. 3**), dKeima responded as fluorescence decrease at the low negative voltage (> ~-1.4V), which was then followed by robust transient of fluorescence increase at the large negative voltage (< ~-1.4V; **Fig. 5a, b**). In the resting electrode, on the other hand, slight fluorescence decrease was observed only at the large negative voltage (**Fig. 5c, d)**. Considering the opposite pH sensitivities in Venus and dKeima, these results clearly indicated that signal interferences by from the light scattering seemed nominal and that the minor responses at the resting electrodes are essentially contributed by the secondary effect, local pH change associated with the HER at the neighboring active electrode. Thus, it was revealed that the secondary effect may spread for ~10um range, producing signals of less than 10% amplitude of that at the active electrode and the polarity of the resultant signal depends on the type of fluorescence protein. From above mentioned data, we concluded that fluorescence protein emission serves as an excellent optical indicator for the spatiotemporal visualization of HER activities of at the metal-solution interface.

Propagating nature of HER activities at the inhomogeneous interfaces

As proof of concept, we then sought to analyze spatio-temporal dynamics of HER at the electrodes with or without a patterned catalysis layer. To this end, we fabricated a star- or a ring-shaped island of platinum/palladium (Pt/Pd) thin layer as electro-catalyst onto the normal bare gold electrodes (**Fig. 6a)**. As a HER indicator, we used dKeima since it allows more straightforward interpretation of the direct and secondary effects than Venus. **Figure 6b** and **6c** show representative responses of electrode currents and total fluorescence, respectively, elicited by the potential scan down to -1.4 V. HER-derived electrode current was less than 100 nA in the bare gold electrode whereas was more than three-fold enhanced in the electrodes with Pt/Pd islands, validating their electro-catalytic function (**Fig. 6b**). Total dKeima fluorescence from the bare gold electrode, during its partial activation of HER, responded as a slight decrease of fluorescence, thus reflecting the secondary effect. This result was totally consistent to the data in **Figure 3** around at the negative voltage down to -1.4V. In the electrodes with Pt/Pd islands, robust increase of total fluorescence was observed, indicating that the direct deprotonation effect serves as the major determinants for dKeima signal during the enhanced HER activities. While the current as well as the total fluorescence profiles are almost identical in the two arrangements (i.e., star & ring) of the Pt/Pd catalyst (**Fig. 6b, c**), dKeima imaging clearly

revealed HER activation pattern which is keenly dependent on the catalyst arrangements (**Fig. 6d**). Emergence of HER active region was initially detected as fluorescence decrease around at the Pt/Pd islands, which was followed by fluorescence increase, therefore showing the initial change in the local pH and subsequent development of the direct deprotonation effect. Moreover, dKeima imaging revealed a notable feature that HER active regions spread over the gold surface, in both star- and ring-shaped Pt/Pd arrangements, from the proximal to the distal locations with respect to the Pt/Pd island. Such propagating nature was reproducibly observed even after replacing the counter and reference electrodes to the different positions in the recording bath, showing that the propagation is not explained by the residual potential gradient across the bath solution. Finally, using the same types of electrodes, Venus was also tested as an HER indicator. While the direct and secondary effects are not readily discriminated against in Venus imaging, the results were all consistent to the interpretation in dKeima imaging. The propagating nature of HER activity was also clearly visualized in HER imaging with Venus.

Discussion

The present study demonstrated high correlations, both in the spatial and temporal aspects,

between HER and the fluorescence protein emission at the metal-solution interface. Fluorescence protein may therefore serve as a unique molecular indicator enabling HER imaging at the near neutral condition. The optical signal is generated through the two HER-driven mechanisms: the direct metal-protein interaction as well as the local-pH mediated alterations of the protein protonation/deprotonation states. During the potential scan, the latter mechanism normally occurs at smaller negative voltage than the former, which was distinguished by using a fluorescence protein with the inverse sensitivity to external pH (e.g., dKeima).

Spatially-resolved detection of local electro-catalytic activities has been expected to provide crucial information to understand and develop efficient reaction environments in two dimensional systems. The scanning electrochemical technique is one of the promising approaches to this end. There have been a variety of the scanning techniques, including the scanning electrochemical microscopy (SECM), the atomic force microscopy combined SECM (AFM-SECM), the scanning electrochemical cell microscopy (SECCM), as well as the micro-droplet cell technique. These enable precise mapping of electrochemical activities at the sub- to several micrometers spatial resolutions (5, 6). The comparison of the present fluorescence protein-based approach with such established scanning techniques clearly highlights the limitations and advantages. One significant

point should be that, while visualizing HER activity based on fluorescence emission is obviously less quantitative and of lower spatial resolution than that based on the scanning electrochemical probes, the fluorescence approach permits detection of HER activities simultaneously over the wide field of view without the need of reconstruction after repeating scans. Accordingly, the present optical and the existing scanning electrochemical approaches provide complementary information of the interfacial HER activities in the two-dimensional systems.

References

1. H.B. Gray, Nat. Chem. 1, 7 (2009).
2. I. Staffell, D. Scamman, A. Velazquez Abad, P. Balcombe, P.E. Dodds, P. Ekins, N. Shah, and K.R. Ward, Energy Environ. Sci. 12, 463 (2019).
3. N. Dubouis and A. Grimaud, Chem. Sci. 10, 9165 (2019).
4. K.E. Clary, M. Karayilan, K.C. McCleary-Petersen, H.A. Petersen, R.S. Glass, J. Pyun, and D.L. Lichtenberger, Proc. Natl. Acad. Sci. U. S. A. 117, 32947 (2021).
5. K. Jaouen, O. Henrotte, S. Campidelli, B. Jousselme, V. Derycke, and R. Cornut, Appl. Mater. Today 8, 116 (2017).
6. Y. Takahashi, Y. Kobayashi, Z. Wang, Y. Ito, M. Ota, H. Ida, A. Kumatani, K. Miyazawa, T. Fujita, H. Shiku, Y.E. Korchev, Y. Miyata, T. Fukuma, M. Chen, and T. Matsue, Angew. Chemie - Int. Ed. 59, 3601 (2020).
7. T. Kogure, S. Karasawa, T. Araki, K. Saito, M. Kinjo, and A. Miyawaki, Nat. Biotechnol. 24, 577 (2006).
8. H. Katayama, T. Kogure, N. Mizushima, T. Yoshimori, and A. Miyawaki, Chem. Biol. 18, 1042 (2011).

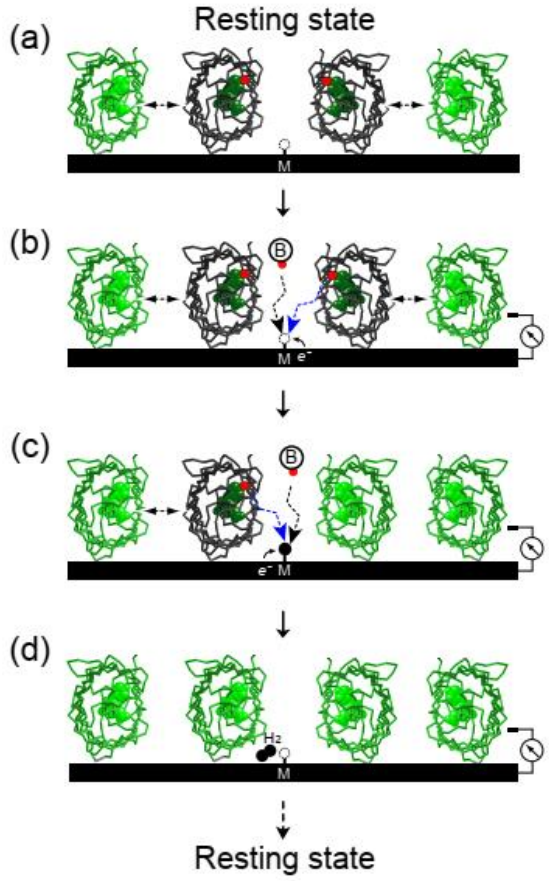

Figure 1. Fluorescence protein emission as an indicator of HER.

(a) The titratable groups in the fluorescence protein at the metal-solution interface, including the chromophore's hydroxyl group, are in the in the equilibrium of protonation/deprotonation. The red circle and "B" indicate proton and buffer in the solution, respectively. **(b, c)** Upon an application of negative voltage, proton adsorption to the metal (M) and reduction become energetically favored, shifting the equilibrium to deprotonations. Buffer and hydronium ions also competitively act as proton source. **(d, e)** The metal-hydrogen pair accepts additional proton to form molecular hydrogen, further facilitating deprotonation. The original equilibrium state is directed upon the removal of the bias.

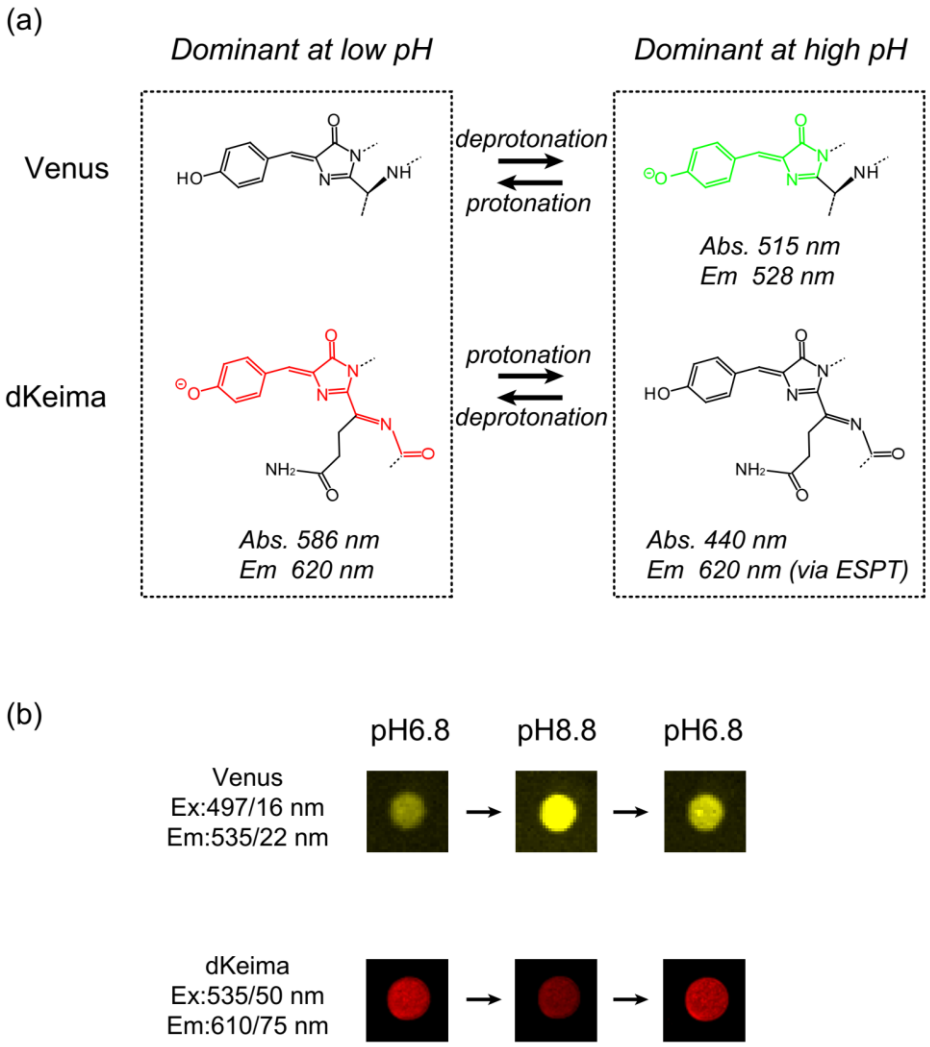

Figure 2. pH dependency of the fluorescence from Venus and dKeima (a) Summary of protonation-deprotonation equilibrium trend of Venus and dKeima known in the bulk (i.e. protein solution) environment. (b) Fluorescence images of ~ϕ50μm circular electrodes immobilized with Venus or dKeima at the metal-solution interface. The buffer solution was changed from 6.8 to 8.8 then back to 6.8.

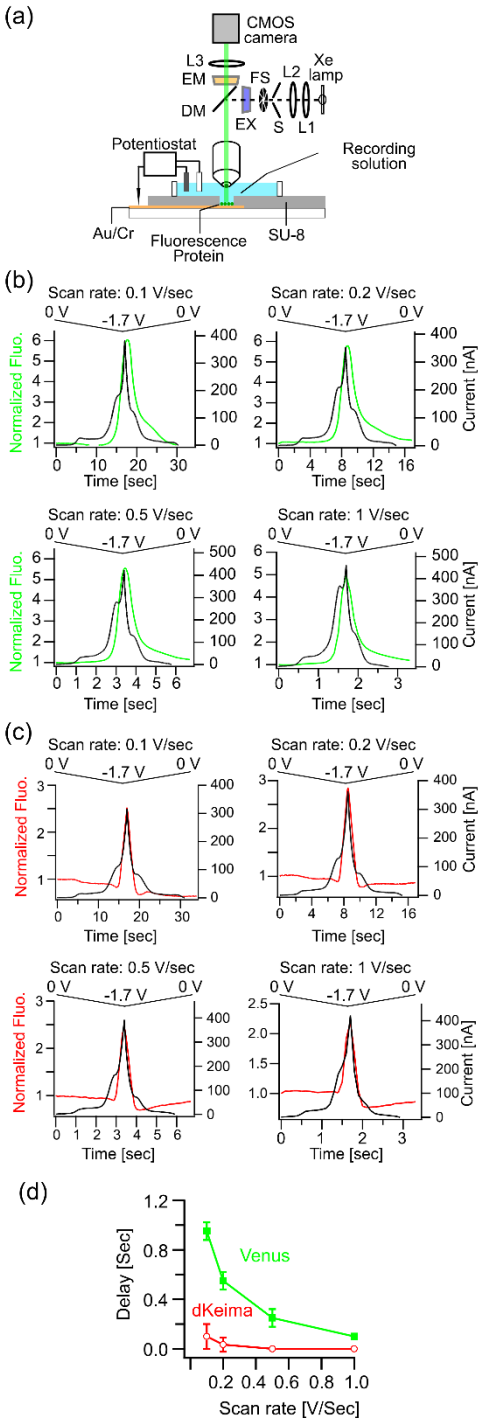

Figure 3. Spatial correlation between HER and fluorescence protein emission at the interface. (a) A scheme of experimental setup. (b) Time course of the current and Venus fluorescence signals elicited by the potential scan from 0 to -1.7 V at the four different rates. (c) The current and dKeima responses at the four scan rates. (d) A plot showing time delay of the optical signal with respect to the current responses in Venus and dKeima at the different scan rates.

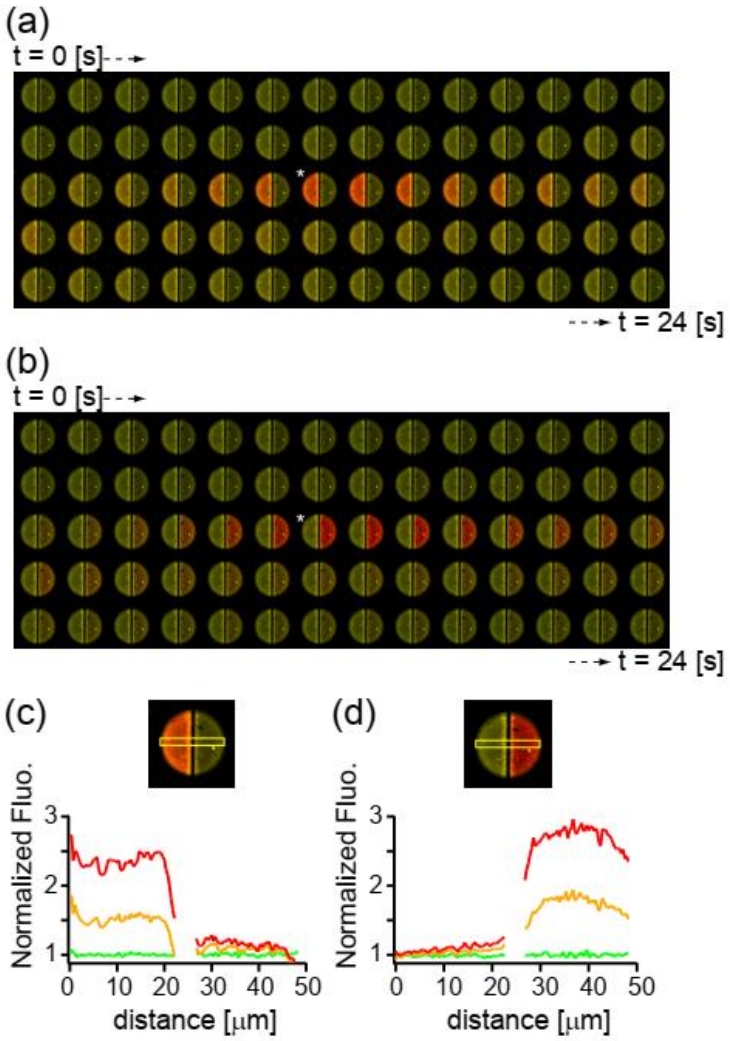

Figure 4. Temporal correlation between HER and fluorescence emission from Venus at the interface. (a, b) A representative response of Venus fluorescence elicited by the potential scan at the left (a) or right (b) electrode. The asterisks indicate the image frames at the negative peak potential (-1.7V). (c, d) Profiles of the fluorescence response along the horizontal axis in the region indicated by the yellow line. The left and right is the active electrode in (c) and (d), respectively.

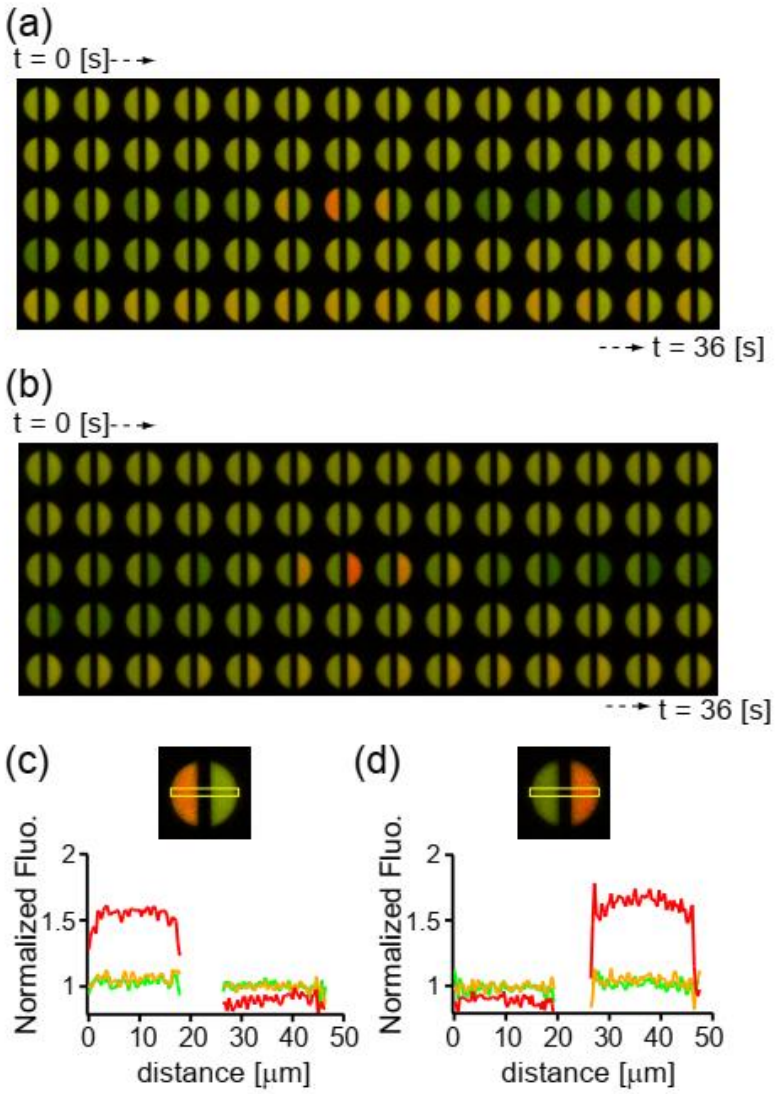

Figure 5. Temporal correlation between HER and fluorescence emission from dKeima at the interface. (a, b) A representative response of Venus fluorescence elicited by the potential scan at the left (a) or right (b) electrode. The asterisks indicate the image frames at the negative peak potential (-1.7V). (c, d) Profiles of the fluorescence response along the horizontal axis in the region indicated by the yellow line. The left and right is the active electrode in (c) and (d), respectively.

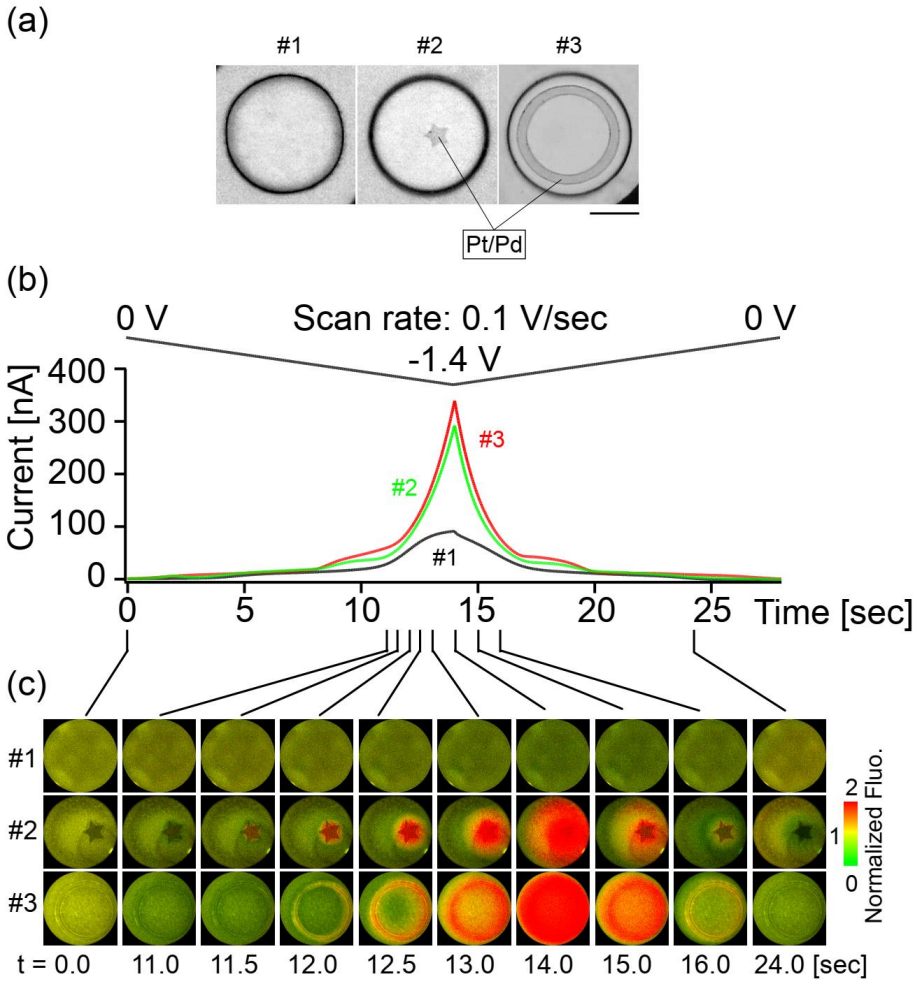

Figure 6. HER imaging at the electrodes with a Pt/Pd pattern as catalysis.

(a) An example of plain electrode (#1), electrodes with a star (#2) or ring (#3) shaped Pt/Pd layer as catalysis. Bar = 20 μm. (b) Representative current responses for the three electorode types #1, 2, and 3 in response to the potential scan from 0 to -1.4V. (c) Representative dKeima responses in the three types of the electrode.

Conclusive Remark

In the 1960s, during the analysis of the properties of a bioluminescent protein that emit blue light, called aequorin, another protein was also isolated from Aequorea victoria jellyfish, and that another protein was called the Green Fluorescent Protein (GFP). GFP-like fluorescent proteins have been discovered in other organisms including corals, copepods, sea anemones, lancelets, zoanithids. GFP can be modified because the genetic code and amino acid code are well known. Modifications allow for GFP to fluoresce with different colors such as blue (BFP), yellow (YFP), cyan (CFP), red (RFP). Previously researches on fluorescent proteins are mainly done in cellular or solution environments. Uncommon environments like surface and interface have been hardly explored. To explore the behavior of fluorescent proteins in such uncommon environments, in this research work, fluorescent proteins are immobilized at a metal-solution interface. After immobilization of fluorescent protein, it was found that the fluorescence protein emission is strongly modulated by the metal potential change to the solution, which was brought out during developing the experimental protocols for electrostatic deposition of protein to the metal substrate. Several experiments have been done to elucidate the potential

dependent manner of modulation of fluorescence emissions. Through this study, it has been known that fluorescent proteins show voltage-dependent modulation at the metal-solution interface after immobilization. It was then desired to solve the mechanism for the cathodic enhancement utilizing the characteristic optical properties of three different fluorescent proteins with showing conventional sensitivity of pH, inverse sensitivity of pH, and green to red photo-convertibility. From simultaneous electrochemical and fluorescence measurements in Venus, a strong correlation between the fluorescence modulation and the current reflecting cathodic hydrogen evolution was observed, which led to a hypothesis that shift in the protonation-deprotonation equilibrium of the chromophore driven by hydrogen evolution at the metal surface underlies the phenomena. And the critical factor for Venus fluorescence that is its hydroxyl group in its chromophore only in a deprotonated state causes Venus fluorescence. So, it can be hypothesized that the negative bias directs the equilibrium toward the direction of deprotonation. Interface-specific mechanism-based possible applications are then discussed, including monitoring of hydrogen evolution reactions at near-neutral conditions.

Acknowledgements

First and foremost, I would like to express my heartfelt and sincere gratitude to Almighty Allah.

My regards and gratitude goes to my supervisor Professor Dr. Hidekazu Tsutsui, Area of Bioscience and Biotechnology (JAIST) for his tremendous support, generosity, patience, and kind advice during my doctoral course.

My extreme thanks go to my minor research supervisor Professor Dr. Yuichi Hiratsuka, Area of Bioscience and Biotechnology (JAIST), for giving me technical support in his lab.

My special thanks go to my Second supervisor Professor Dr. Goro Mizutani, Area of Applied Physics (JAIST).

My deep thanks go to my lab member Mrs. Mieko Imayasu for her great support in my research work.

I would like to thank my University, JAIST, for giving me Doctoral research Fellowship (DRF).

Many thanks go to all my lab members. Special thanks go to my Lab mate Mr. Kohsuke Hama, Mr. Kim Samyoung and Mr. SM. Ahasanul Hamid and others.

Finally, and most importantly, I express my deepest gratitude and love to my Parents and family members.

JAIST, March 2023

TRISHA FARHA DIBA